
1

SOLID PROPELLANTS AND THEIR COMBUSTION CHARACTERISTICS

SYMBOLS

Symbol	Description	Dimension
A_e	Exit area of a rocket nozzle	L^2
A_s	Arrhenius factor in Equation 1.27	$(L/t)/(T)^\beta$
A_t	Throat area of the rocket nozzle	L^2
a	Coefficient used in Saint-Robert's burning rate law (or Vieille's Law)	$(L/t)/(F/L^2)^n$
C_D	Mass flow factor defined in Equation 1.50	t/L
C_F	Dimensionless thrust coefficient	—
C_p	Constant-pressure specific heat	$Q/(MT)$
C^*	Characteristic velocity, defined in Equation 1.62	L/t
DI_{sp}	Density impulse defined in Equation 1.60	Mt/L^3
E_a	Activation energy in the Arrhenius law of Equation 1.24	Q/N
F	Thrust force of a solid propellant rocket	F
F_e	Net force acting on the exterior surface of a rocket motor	F
F_i	Net force acting on the interior surface of a rocket motor	F
I_f	Radiative energy flux	$Q/(L^2t)$
I_m	Impetus of a gun propellant	Q/M
I_{st}	Specific impulse	t

Symbol	Description	Dimension
I_t	Total impulse of a rocket	Ft
K_n	Ratio of propellant burning surface area to throat area	—
k_f	Specific reaction-rate constant (for a forward reaction of order of m)	$(N/L^3)^{1-m}/t$
k_g	Thermal conductivity of gas	Q/(LTt)
k_p	Thermal conductivity of propellant	Q/(LTt)
\mathcal{L}	Dynamic vivacity, defined in Equation 1.96	$L^2/(Ft)$
L_w	Web thickness	L
M	Mass	M
M_i	The i^{th} molecular species	—
M_w	Molecular weight of the combustion products	M/N
\dot{m}_p	Propellant mass burning rate per unit area	$M/(L^2t)$
N	Total number of chemical species	—
n	Pressure exponent of Saint-Robert's law (or Vieille's law)	—
P or p	Pressure	F/L^2
P_c	Pressure in the rocket motor combustor	F/L^2
Q_g	Heat of reaction per unit mass	Q/M
Q_s	Heat release per unit mass at burning propellant surface	Q/M
\dot{q}_r	Radiative heat flux	$Q/(L^2t)$
r_b	Burning rate of solid propellant	L/t
R	Gas constant	$Q/(MT)$
RF	Relative force, defined in Equation 1.93	—
RQ	Relative quickness, defined in Equation 1.92	—
R_u	Universal gas constant	$Q/(NT)$
T	Temperature	T
T_i	Initial temperature	T
T_s	Surface temperature of a burning propellant	T
t	Time	t
U	Internal energy	Q
U_g	Gas velocity	L/t
\mathcal{V} or V	Volume	L^3
V_e	Exhaust jet velocity from a rocket motor, or muzzle velocity	L/t
$V_{e,vac}$	Effective vacuum exhaust jet velocity of a rocket motor	L/t
W	Work	Q
X_k	Mole fraction of the k^{th} species	—
x	Distance measured away from burning propellant surface	L

Symbol	Description	Dimension
Y_i	Mass fraction of i^{th} species, defined in Equation 2.59	—
y	Subsurface distance normal to the burning surface of a propellant	L
Greek Symbols		
α_d	Divergence angle of the nozzle exit station measured from centerline	°
α_p	Thermal diffusivity of solid propellant	L ² /t
β	Dimensionless temperature exponent, defined in Equation 1.27	—
Γ	Dimensionless parameter defined in Equation 1.44	—
δ_{th}	Thermal wave thickness	L
ΔH_{ex}^o	Heat of explosion per unit mass, defined in Equation 1.91	Q/M
ε	Strain	—
ζ_e	Characteristic coefficient of a gun system	—
η_b	Ballistic efficiency, defined in Equation 1.85	—
η_{C_F}	Thrust coefficient efficiency, defined in Equation 1.71	—
η_p	Piezometric efficiency, defined in Equation 1.83	—
η_{th}	Thermal efficiency of a gun system, defined in Equation 1.88	—
θ	Dimensionless temperature defined in Equation 1.5	—
Λ	Ratio of propellant mass to rocket motor mass	—
λ	Parameter associated with the divergence angle of the nozzle exit section, defined in Equation 1.40	—
v_i'	Stoichiometric coefficient of the i^{th} reactant	— or N
v_i''	Stoichiometric coefficient of the i^{th} product	— or N
π_k	Pressure insensitivity of the rocket motor, defined in Equation 1.66	1/T
ρ	Density	M/L ³
σ_p	Temperature sensitivity of a propellant	1/T
τ	Stress	F/L ²
$\dot{\omega}_g'''$	Gas-phase reaction rate per unit volume	M/(L ³ t)
Subscripts		
f	Forward reaction	
g	Gas	
i	Initial or i^{th} species	
p	Propellant	
s	Surface	

Many books are specifically devoted to solid propellants. Readers interested in extensive discussions of solid propellant combustion can read the books edited by Kuo and Summerfield (1984), De Luca, Price, Summerfield (1992), Yang, Brill, and Ren (2000), and Kubota (2007). This chapter provides the background information for readers to understand certain basic materials related to the solid propellants and their combustion characteristics.

The chapter includes performance parameter considerations for solid propellant rocket motors and gun propulsion systems. Definitions and significance of many important parameters for rocket motors are covered at the beginning of the chapter, including specific impulse, characteristic velocity, thrust coefficient, density Isp, pressure sensitivity parameter, thrust-coefficient efficiency, and others. Various performance parameters for solid-propellant gun systems are also covered, including muzzle velocity, pressure-travel curve, maximum pressure, velocity-travel curves, piezometric efficiency, ballistic efficiency, gun-propellant impetus, thermal efficiency, characteristic coefficient, relative quickness, relative force, and dynamic vivacity. Many of these parameters have been considered in the formulation and development of modern solid propellants for both rocket and gun propulsion systems for space propulsion and military applications. The chapter also addresses the relationship between propellant burning rate behavior and these performance parameters.

1.1 BACKGROUND OF SOLID PROPELLANT COMBUSTION

1.1.1 Definition of Solid Propellants

A solid propellant is a solid state substance that contains both oxidizer and fuel and is able to burn in the absence of ambient air. Solid propellants usually generate a large number of gaseous molecules at high temperatures ($T_f = 2,300\text{--}3,800\text{ K}$) during combustion. Condensed phase species are produced, especially from metallized solid propellants. High-temperature combustion products are used mainly for propulsion and gas generation purposes. There are two types of solid propellants, which are differentiated by the condition in which their ingredients are connected:

1. In *homogeneous propellants*, the oxidizer and fuel are chemically linked and form a single chemical structure. These propellants are physically homogeneous.
2. In *heterogeneous propellants*, the oxidizer and fuel are physically mixed but do not have chemical bonds between them. These propellants are physically heterogeneous.

1.1.2 Desirable Characteristics of Solid Propellants

- High gas temperature and/or low molecular mass of products
- High density

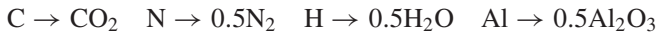
- Good mechanical and bond properties
- Good aging characteristics
- Desirable ignition characteristics (to be addressed later)
- Low-hazard manufacturing and handling
- Predictable and reproducible properties (mechanical, burning rate, etc.)
- Low thermal expansion coefficient
- Low temperature sensitivity
- Nontoxic exhaust gases with minimum smoke
- Low absorption of moisture
- Minimum sensitivity of burning velocity to pressure, initial temperature, and gas velocity (erosive burning)

1.1.3 Calculation of Oxygen Balance

The oxygen balance of a propellant is the amount of oxygen in weight percentage that is liberated as a result of complete conversion of the energetic material into CO_2 , H_2O , SO_2 , Al_2O_3 , and others. If the equilibrium products of a propellant contain an excess amount of oxygen, the oxygen balance of this propellant is positive. If oxygen is needed for the complete combustion of the energetic material (EM), the oxygen balance is negative. Usually the oxygen balance of a solid propellant is negative. Oxygen balance is defined as:

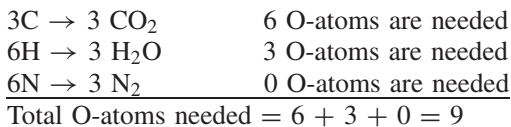
$$\text{OxygenBalance} = \frac{\text{Mass of excess oxygen in 1 mole of compound}}{\text{Mass of 1 mole of compound}} \quad (1.1)$$

The calculation of oxygen balance is performed by assuming the conversion of the atoms (like C, H, N, O, and Al, etc.) into fully oxidized molecules:



EXAMPLE 1.1

RDX ($\text{C}_3\text{H}_6\text{O}_6\text{N}_6$); Calculate the oxygen balance of which is a propellant ingredient that also can be considered a monopropellant for its oxygen balance calculation.



For a complete combustion, 9 oxygen atoms are needed. The RDX molecule supplies 6 atoms, which means that 3 atoms are still required. The molecular weight of 3 g-atoms of oxygen is equal to $3 \times 15.9994 = 47.998$ g. The molecular weight of the RDX compound is 222.117 g, which corresponds to 100%; $47.998 \text{ g} \div 222.117 \text{ g} = 0.2161$. Therefore, the oxygen balance of RDX is -21.61% .

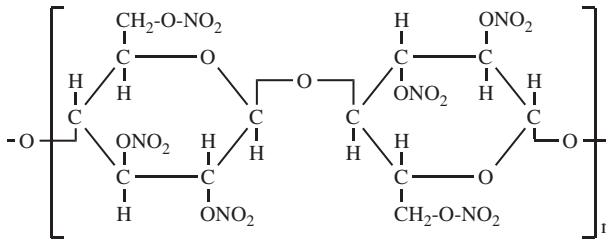
Note: In case a compound contains Cl, consider $\text{H} + \text{Cl} \rightarrow \text{HCl}$ as the reaction.

1.1.4 Homogeneous Propellants

Homogeneous propellants have a uniform physical structure consisting of chemically bonded fuel and oxidizer ingredients. Their major constituents are nitrocellulose (NC) and nitroglycerine (NG). Nitrocellulose is a typical example of single-base homogeneous propellants. Nitrocellulose is a nitrated cellulose whose chemical structure is represented by $C_6H_{7.55}O_5(NO_2)_{2.45}$ and $C_6H_{7.0006}N_{2.9994}O_{10.9987}$ for 12.6% and 14.14% nitrogen content, respectively. Propellants that are composed of NC and NG are called double-base propellants and are typical homogeneous propellants. The molecular structures and thermochemical properties of several homogeneous propellant ingredients are shown in Figures 1.1 to 1.3.

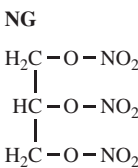
1.1.4.1 Decomposition Characteristics of NC

When nitrocellulose is decomposed thermally, two major fragments are generated. One group of fragments with a C/H and C/H/O structure acts as a fuel with the other fragment of NO_2 acting as an oxidizer. Since nitrocellulose is a fibrous material, it is difficult to form a specified propellant grain using it as a single ingredient (called monopropellant). Liquid materials called plasticizers usually are mixed with the nitrocellulose to gelatinize it and to form a specific shape for



Nitration level	14.14%
Molecular weight	297.106 g/mol
Oxygen balance	-24.24%
Density	1.66 g/cc
Heat of combustion	650.6 kcal/mol
Enthalpy of formation	-155.99 kcal/mol
Physical state	Solid

Figure 1.1 Molecular structure and thermochemical properties of nitrocellulose (NC).



Nitration level	-
Molecular weight	227.087 g/mol
Oxygen balance	3.52%
Density	1.593 g/cc
Heat of combustion	364.3 kcal/mol
Enthalpy of formation	-84.90 to -118.90 kcal/mol
Physical state	Liquid

Figure 1.2 Molecular structure and thermochemical properties of nitroglycerine (NG).

TMETN	
$ \begin{array}{c} \text{CH}_2\text{-O-NO}_2 \\ \\ \text{CH}_3\text{-C-CH}_2\text{-O-NO}_2 \\ \\ \text{CH}_2\text{-O-NO}_2 \end{array} $	Nitration level - Molecular weight 255.141 g/mol Oxygen balance -34.49% Density 1.488 g/cc Heat of combustion 674.0 kcal/mol Enthalpy of formation -92.90 to -113.80 kcal/mol Physical state Liquid
DEGDN	
$ \begin{array}{c} \text{CH}_2\text{-O-NO}_2 \\ \\ \text{CH}_2 \\ \\ \text{O} \\ \\ \text{CH}_2 \\ \\ \text{CH}_2\text{-O-NO}_2 \end{array} $	Nitration level - Molecular weight 196.117 g/mol Oxygen balance -40.79% Density 1.385 g/cc Heat of combustion 548.7 kcal/mol Enthalpy of formation -99.40 to -113.80 kcal/mol Physical state Liquid

Figure 1.3 Molecular structure and thermochemical properties of trimethylolethane trinitrate (TMETN) and diethylene glycol dinitrate (DEGDN).

the propellant grain. Typical examples of plasticizers include nitroglycerin (NG) and trimethylolethane trinitrate (TMETN). Both NG and TMETN are also nitrated materials which can function individually as propellants in the liquid form.

1.1.5 Heterogeneous Propellants (or Composite Propellants)

Heterogeneous (composite) propellants have a non-uniform physical structure (see Figures 1.4 and 1.5). The fuel usually has a polymeric hydrocarbon structure, such as hydroxyl-terminated polybutadiene (HTPB). The fuel has a dual function:

1. To produce energy when burned with oxidizer-rich species
2. To bind the oxidizer particles together to form a specified propellant grain shape

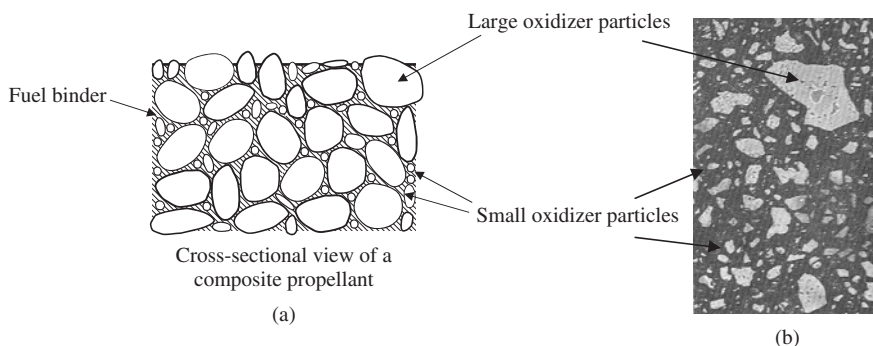


Figure 1.4 (a) Cross-sectional view of a composite propellant and (b) a photograph of the top view of an AP-based solid propellant with ~65 wt% AP loading (modified from Summerfield et al., 1960).

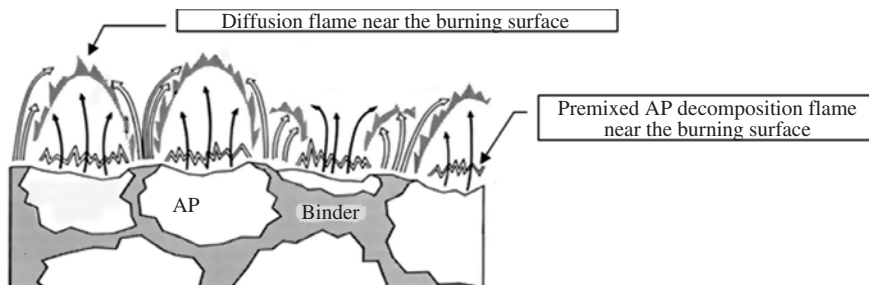


Figure 1.5 Flame structure of ammonium perchlorate (AP)-based composite propellant.

The organic fuel material is initially in a liquid or semiliquid form that can be cured to form a solid.

Composite propellants usually are made of a polymeric matrix, loaded with a solid powder oxidizer and possibly a metal powder (e.g., aluminum) that plays the role of a secondary (but highly energetic) fuel component. In composite propellants, the oxidizer and fuel containing molecules come from separate components. Therefore, the flame structure is three dimensional and nonpremixed (see Figure 1.5).

The major propellant properties, such as burning rate, rheology, and mechanical behavior, are directly dependent on the size and distribution of fuel and oxidizer particles in the composite propellant matrix. Oxidizer and metallic fuel ingredients are usually in the form of solid powders, which must be mixed with a binder to provide cohesion and even distribution.

1.1.6 Major Types of Ingredients in Solid Propellants

A solid propellant consists of several different types of ingredients. Each of these ingredients serves a specific function. The most common ingredients are shown in Table 1.1 for homogeneous propellants and in Table 1.2 for heterogeneous propellants. Molecular structures of certain ingredients that are used in propellants and explosives are shown in Figure 1.6. The functions of propellant ingredients is described next.

- **Oxidizer.** Usually crystalline particles to supply oxygen-rich species.
- **Fuel binder.** Liquid-form hydrocarbon polymers to hold the solid oxidizer particles together and provide fuel-rich component for burning. It also controls the mechanical properties.
- **Plasticizer.** For obtaining superior characteristics of grain formation, to improve mechanical properties, and to reduce shock sensitivities.
- **Stabilizer.** For increasing chemical stability of composite solid propellants.
- **Curing agent and/or cross-linking agent.** For curing the prepolymers in the binder material and forming chemical bonds between the binder materials.

TABLE 1.1. Ingredients Used in Homogeneous Propellants

Ingredient	Examples
Plasticizer (fuel and oxidizer)	NG: nitroglycerin TMETN: trimethylolthane trinitrate TEGDN: triethylene glycol dinitrate DEGDN: diethylene glycol dinitrate
Plasticizer (fuel)	DEP: diethylphtalate TA: triacetine PU: polyurethane
Binder (fuel and oxidizer)	NC: nitrocellulose
Stabilizer	EC: ethyl centralite 2NDPA: 2-nitrodiphenilamine
Burning rate catalyst	PbSa: lead salicylate Pb ₂ EH: lead 2-ethylhexoate PbST: lead stearate CuSa: copper salicylate CuSt: copper stearate LiF: lithium fluoride
High-energy additive	RDX: cyclotrimethylene trinitramine HMX: cyclotetramethylene tetranitramine NGD: nitroguanidine
Coolant	OXM: oxamide
Opacifier	C: carbon black
Flame suppressant	KNO ₃ : potassium nitrate K ₂ SO ₄ : potassium sulfate
Metal fuel	Al: aluminum
Combustion instability suppressant	Al: aluminum Zr: zirconium ZrC: zirconium carbide

The cross-linking agent helps to form long chains and complex three-dimensional polymers.

- **Bonding agent**. Used to increase the adherence of each oxidizer particle to the binder.
- **Burning rate catalyst**. For increasing (or sometimes decreasing) the burning rate of solid propellants.
- **Antiaging agent**. Used to prevent deterioration of the propellant physical properties with time.
- **Opacifier**. Used to make the propellant less translucent so that in-depth radiation absorption is avoided.

TABLE 1.2. Ingredients Used in Heterogeneous Propellants

Type of Ingredient	Examples
Oxidizer	AP: ammonium perchlorate AN: ammonium nitrate NP: nitronium perchlorate KP: potassium perchlorate RDX: cyclotrimethylene trinitramine HMX: cyclotetramethylene tetranitramine
Binder	PBAN: polybutadiene acrylonitrile CTPB: carboxyl terminated polybutadiene HTPB: hydroxyl terminated polybutadiene
Curing and/or cross-linking agents	PQD: paraquinone dioxime TDI: toluene-2,4-diisocyanate MAPO: tris {1-(2-methyl) aziridiny} phosphine oxide ERLA-05I0: N,N,O-tri (1,2-epoxy propyl)-4-aminophenol IPDI: isophorone diisocyanate
Bonding agent	MAPO: tris{1-(2-methyl) aziridiny} phosphine oxide TEA: triethanolamine MT-4: adduct of 2.0 moles MAPO, 0.7 mole azipic acid, and 0.3 mole tararic acid
Plasticizer	DOA: dioctyl adipate IDP: isodecyl pelargonete DOP: dioctyl phthalate
Burning rate catalyst	Fe ₂ O ₃ : ferric oxide FeO(OH): hydrated-ferric oxide nBF: n-butyl ferrocene DnBF: di-n-butyl ferrocene
Metal fuel	Al: aluminum
Combustion instability suppressant	Al: aluminum Zr: zirconium ZrC: zirconium carbide

- **Flame suppressant**. For suppressing the flame luminosity.
- **Combustion instability suppressant**. For reducing the burning rate sensitivity to pressure fluctuations.

1.1.6.1 Description of Oxidizer Ingredients

Oxidizer ingredients usually have positive oxygen balance, as shown in Table 1.3 for many commonly used oxidizers. Among them, ammonium perchlorate (AP, with a chemical formula of NH₄ClO₄) is the most widely used oxidizer. It is

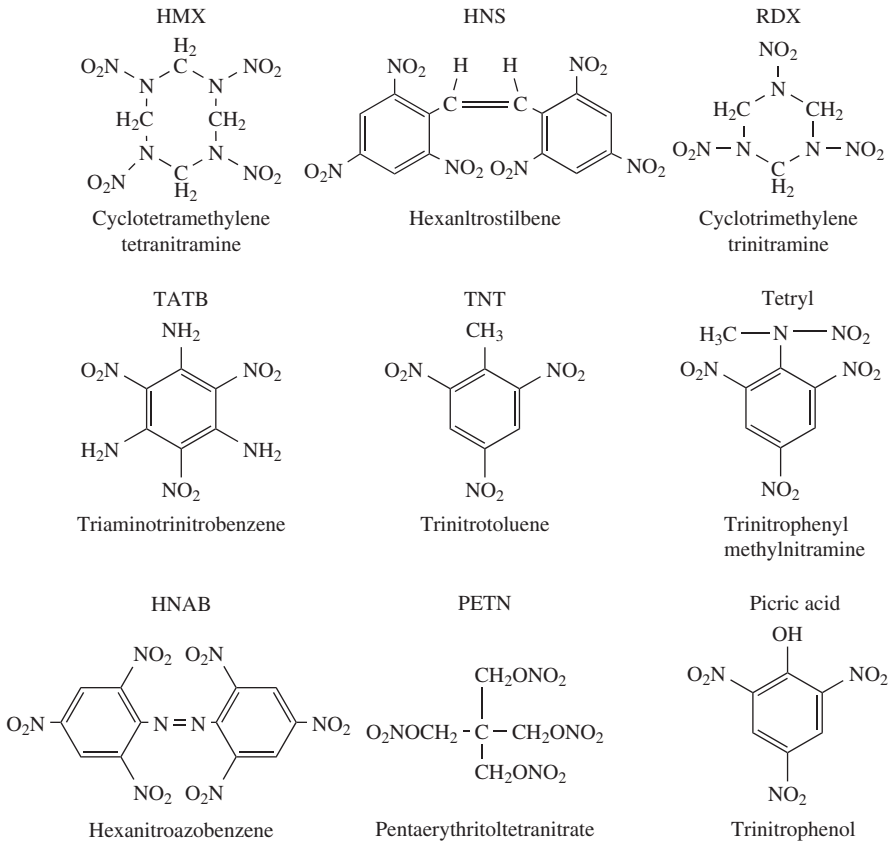


Figure 1.6 Molecular structures of selected explosive or propellant ingredients.

TABLE 1.3. Properties of Several Solid Oxidizers

Oxidizer	Molecular Formula	Melting/ Decomposition Temperature (K)	ΔH_f^0 (kJ/mol)	Density (Kg/m ³)	Oxygen Balance, %
AN	NH ₄ NO ₃	443	-365.04	1720	20.0
AP	NH ₄ ClO ₄	403	-296.00	1950	34.0
HP ₂ [*]	N ₂ H ₆ (ClO ₄) ₂	443	-293.30	2200	41.0
HP [*]	N ₂ H ₅ ClO ₄	443	-177.80	1940	24.0
ADN	NH ₄ N(NO ₂) ₂	363	-150.60	1820	25.8
HNF	N ₂ H ₅ C(NO ₂) ₃	395	-72.00	1870-1930 [†]	13.1
NP [*]	NO ₂ ClO ₄	393	37.10	2220	66.0
RDX	C ₃ H ₆ N ₆ O ₆	477	70.63	1820	-21.6
HMX	C ₄ H ₈ N ₈ O ₈	548	74.88	1960	-21.6

^{*}HP₂ (hydrazine diperchlorate, also known as HP₂), HP (hydrazine perchlorate), and NP (nitryl perchlorate) are extremely unstable and therefore have not been used as oxidizers.

[†]Based on literature data, measurements at PML-TNO gave a density of 1910 kg/m³.

a white crystalline material that is usually orthorhombic but transforms into cubic form at 513 K. It starts to decompose at approximately 470 K according to the next global chemical reaction:



Beyond 620 K, it decomposes according to this global chemical reaction:



When AP is burned with polymeric hydrocarbon fuels, it produces mainly CO_2 , H_2O , N_2 , and HCl . Even though AP has some undesirable features—including the production of HCl for acid rain; groundwater pollution; causing thyroid problems, especially for women; and generation of partially toxic combustion products—it is still widely used for propellants and explosives due to its high oxygen balance and relative stability to mechanical shocks. Because of the drawbacks of AP, one of the current aims of the propellant field is to find a suitable replacement for future applications in space propulsion, military, and commercial areas.

Even though RDX and HMX were initially developed as explosive ingredients, they have been utilized as oxidizers for some solid propellants due to their higher thermal stability, lower toxicity, and lack of HCl production upon combustion.

1.1.6.2 Description of Fuel Binders

The fuel binder provides the structural glue or matrix in which solid granular ingredients (such as oxidizer particles and/or metal fuels) are held together in heterogeneous (composite) propellants. The binder raw materials are liquid prepolymers or monomers. After they are mixed with the solid ingredients, cast, and cured, they form a hard rubberlike material that constitutes the propellant grain. In short, a prepolymer is a molecule formed by the repetition (in several orders of magnitudes) of a monomer form (butadiene, polypropylene oxide, etc.), generally ending with reactive functions (telechelic prepolymers). Binders inherit their essential properties from the prepolymers. These properties can be derived from the nature of the polymeric chain or the properties of the functional group at its ends. The molecular structure of polyether prepolymer is:



A curing agent or cross linker causes the prepolymers to form longer chains of larger molecular mass and interlocks between chains. (It causes the binder to solidify and become hard.) Polymerization occurs when the binder monomer and its cross-linking agent react (beginning in the mixing process) to form long chains and complex three-dimensional polymers. The binder ingredient has important effects on rocket motor reliability, mechanical properties, propellant processing complexity, storability, aging, and costs.

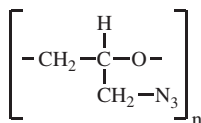


Figure 1.7 Molecular structure of GAP.

1.1.6.2.1 Characteristics of Glycidyl Azide Polymer Binder Glycidyl azide polymer (GAP) is an example of an energetic, thermally stable, hydroxyl-terminated prepolymer that can be polymerized (Sutton and Biblarz, 2001). According to (Bathelt, Volk, and Weindel (2001); and as shown in Figure 1.7, the GAP formulation is:



Molecular weight: 99.092 g/mol

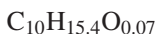
Oxygen balance: -121.09%

Density: 1.29 g/cm³

Melting point: >200°C

Enthalpy of formation: 141.0 kJ/mol (340.09 kcal/kg).

1.1.6.2.2 Characteristics of Hydroxyl-Terminated Polybutadiene Binder Hydroxyl-terminated polybutadiene (HTPB) is the most commonly used prepolymer binder material. It allows a high solid fraction (88% to 90% of AP and Al by mass) and relatively good physical properties at the temperature range from -50° to 65°C (Sutton and Biblarz, 2001). Several different chemical formulae exist for HTPB. A typical one (Bathelt, Volk, and Weindel, 2001) is shown in Figure 1.8:



Molecular weight: 136.752 g/mol

Oxygen balance: -323.26%

Density: 0.916 g/cm³

Melting point: 241°C

Enthalpy of formation: -51.88 kJ/mol (-90.68 kcal/kg)

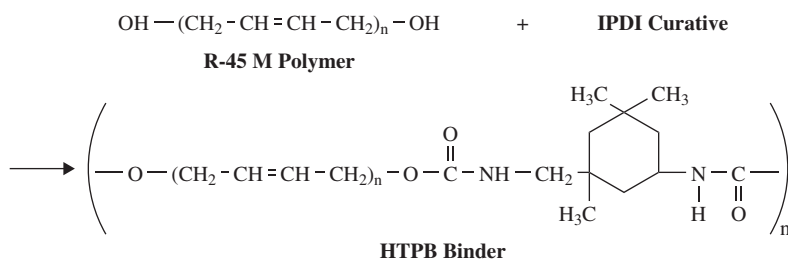


Figure 1.8 Molecular structures of HTPB.

1.1.6.2.3 Desired Properties of a Binder The binder must be in liquid form during the preliminary phase of the preparation of the intimate mixture of oxidizer and fuel ingredients, although its elements must have sufficiently low volatility characteristics to withstand the high vacuum used during the mixing of the slurry and the casting of the propellant into a particular grain shape. It must be chemically compatible with the oxidizer, which means that it will not cause even a slight temperature increase that may result in an exothermic reaction leading to any unwanted autoignition of the propellant. It must be capable of accepting very high solid loading ratios (up to 80% in volume). The mixing operation must remain feasible, and the resulting slurry must be easily cast into the rocket motor case with molding devices of shapes that are often complex and include some very narrow regions. The mechanical properties of the propellant depend strongly on the selected binder.

1.1.6.3 Curing and Cross-Linking Agents

A curing agent or cross-linker causes the prepolymers to form longer chains of larger molecular mass and interlocks between chains. Even though these materials are present in small amounts (0.2 to 3%), a minor change in the percentage can have a major effect on the propellant physical properties, manufacturability, and aging. A curing agent and/or cross-linker are used only with composite propellants. These ingredients cause the binder to solidify and become hard (Sutton and Biblarz, 2001).

The cross-linking agent in its most simple state could be a polyfunctional molecule (frequently trifunctional) with a low molecular weight or a mixture of bifunctional and trifunctional molecules. This approach can ensure an average functionality (i.e., number of reactive functions, divided by the total number of molecules) greater than 2 for the whole cross-linking system. The bifunctional molecules are generally called chain extenders, and their role is to increase the length of the chain of prepolymers. Chemical reaction occurs between the prepolymer and the cross-linking agent after the polymer addition and the three-dimensional links are created (Davenas, 1993). An example of a curing agent is isophorone diisocyanate (IPDI), as shown in Figure 1.9:



Molecular weight: 222.287 g/mol

Oxygen balance: -223.13%

Density: 1.061 g/cm^3

Enthalpy of formation: -372.00 kJ/mol (-399.98 kcal/kg)

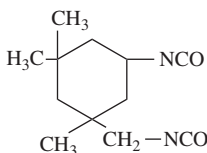


Figure 1.9 Molecular structure of IPDI.

1.1.6.3.1 Desired Properties of a Curing Agent/Cross-Linker After the slurry (mixed oxidizer and prepolymer) is in the casting mold, cross-linking must ensure its transformation into a solid through a chemical reaction that obeys these criteria (Davenas, 1993):

- It must be a polyaddition reaction. Any elimination reaction producing more or less volatile products would result in the creation of cracks or “bubbles” in the cross-linked material. It is extremely important that the slurry mixing is conducted under vacuum to eliminate the gas present in soluble form in the binder. Otherwise, upon heating during the curing process, the gases dissolved in the slurry may lead to bubble or crack formation in the propellant.
- This reaction must have a sufficiently slow cure kinetic rate to allow for the casting operations. This useful reaction time of several hours is also known as the pot life. However, the reaction rate should not be too slow so that it does not require lengthy cross-linking or curing times.
- To prevent severe mechanical loads in case-bonded propellants, the curing temperature cannot be too high.
- The curing process must also be athermic (heatless), or not very exothermic, to avoid the release of heat inside the propellant grain, which can result in a temperature increase inside the propellant. (The propellant usually is a poor heat conductor.) This temperature increase could lead to mechanical loading conditions, possibly leading to cracks and autoignition of the propellant.

1.1.6.4 Aging

The term “aging” when used in regard to solid propellants in rocket motors refers to the deterioration of their physical properties with time. It is caused by the *cumulative damage* to the grain (such as by thermal cycling and load applications) during storage, handling, or transport. It can also be caused by chemical changes with time, such as the gradual depletion (evaporation) of certain liquid plasticizers or moisture absorption. The ability to carry stress or to allow elongation in propellants diminishes with cumulative damage. The *aging limit* is the estimated time when a rocket motor is no longer able to perform its operation reliably or safely. Depending on the propellant and the grain design, this aging limit or motor life can be between 8 and 25 years (Sutton and Biblarz, 2001).

With small tactical rocket motors, the aging limit usually is determined by full-scale motor firings tests at various time periods after manufacture, say two or three years. Accelerated temperature aging (more severe thermal cycles) and accelerated mechanical pulse loads and overstressing often are used to reduce the time needed for these tests (Sutton and Biblarz, 2001). The term “rocket motor aging” refers not only to the propellant but also to other components, such as the igniter’s pyrotechnic charge, initiator material, O-rings and other organic material, and metals.

1.1.7 Applications of Solid Propellants

Solid propellants have been used for both military and commercial purposes. Military applications include missiles, guns, and air-breathing propulsion systems. Commercial applications include, among others, rockets for space explorations, satellite deployment, air bags in automobiles, electric cable connections, emergency airplane crew and passenger escape systems, gas generator systems for fire extinguishers.

1.1.7.1 Hazard Classifications of Solid Propellants

The classification of a given propellant (mostly 1.1 or 1.3) determines the method of labeling and the cost of shipping rocket propellants, loaded military missiles, explosives, or ammunition; it also determines the required limits on the amount of that propellant stored or manufactured in any one site and the minimum separation distance of that site to the next building or site.

1.1.7.1.1 Class 1.1 Propellants that can experience a transition from deflagration to detonation are considered more hazardous and usually are designated as class 1.1-type propellants. With a class 1.1 propellant, a powerful detonation sometimes can occur that rapidly gasifies all the remaining propellant and is much more powerful and destructive than the bursting of the rocket motor case under high pressures. Unfortunately, the term “explosion” has been used to describe both a bursting of a case with fragmentation of the motor and the higher rate of energy release of a detonation, which leads to a very rapid and more energetic fragmentation of the rocket motor.

1.1.7.1.2 Class 1.3 Under normal conditions, most propellants “burn” and do not “detonate.” The rocket motor case may burst when the chamber pressure becomes too high. If the rocket motor case should burst violently with a class 1.3 propellant, then much of the remaining unburned propellant would be thrown out but eventually would stop burning. (Note: “Class 1.2” corresponds to non-mass-detonating and fragment-producing device. “Class 1.4” corresponds to moderate fire, no detonation, and no fragment.)

1.1.8 Material Characterization of Propellants

1.1.8.1 Propellant Density Calculation

For a propellant with multiple components (N_c components in total), the density can be calculated from the mass fraction and the densities of individual components by this equation:

$$\rho_{propellant} = \frac{1}{\sum_{j=1}^{N_c} \frac{Y_j}{\rho_j}} \quad (1.2)$$

EXAMPLE 1.2

Evaluate the density of two propellants containing following components:

Component	Name	Mass Fraction, Y_j	ρ , (g/cm ³)
1.	HTPB	0.12	0.918
2.	AP	0.88	1.950

$$\left. \vphantom{\begin{matrix} 1. \\ 2. \end{matrix}} \right\} \rho_{\text{propellant}} = 1.718 \text{ g/cm}^3$$

Component	Name	Mass Fraction, Y_j	ρ , (g/cm ³)
1.	HTPB	0.12	0.918
2.	AP	0.70	1.950
3.	Al	0.18	2.700

$$\left. \vphantom{\begin{matrix} 1. \\ 2. \\ 3. \end{matrix}} \right\} \rho_{\text{propellant}} = 1.797 \text{ g/cm}^3$$

1.1.8.2 Propellant Mass Fraction, Λ

The propellant mass fraction, Λ , is a measure of motor design loading efficiency. As shown in Equation 1.3, it usually is defined as the ratio of the mass of initial propellant to the mass of the total rocket motor, where the total motor consists of the initial propellant plus motor inert components (motor case, nozzle assembly, etc.).

$$\Lambda \equiv \frac{M_{\text{Propellant}}|_{t=0}}{M_{\text{Rocket Motor}}|_{t=0}} \tag{1.3}$$

Solid-propellant mass fractions vary from about 0.3 to 0.96. The lower values apply to auxiliary motors, gas generators, and very small motors; the high mass fractions apply to simple motors and particularly upper-stage motors.

1.1.8.3 Viscoelastic Behavior of Solid Propellants

The solid propellant is a rubberlike material that is nearly incompressible. Usually there are very few voids ($\gg 1\%$) in a properly made propellant. However, propellants are easily damaged by applied tension and shear loads. These types of stress loads can cause damage due to the “dewetting” of the adhesion between individual oxidizer particles and the binder material surrounding them. Under vacuum conditions, very small voids can exist next to the oxidizer particles. These voids can become larger with increase of shear or tensile strains. Propellants usually show a nonlinear viscoelastic behavior. The stress in solid propellants is a

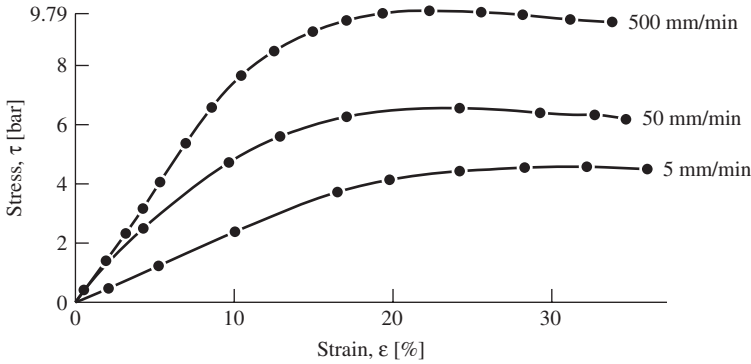


Figure 1.10 Effect of strain rate on viscoelastic behavior of solid propellants.

function not only of strain but also of the strain rate, as shown by Equation 1.4 and the curves in Figure 1.10.

$$\tau = f\left(\varepsilon, \frac{d\varepsilon}{dt}\right) \quad (1.4)$$

The nonlinear mechanical behavior means that the stress response of propellants depends on both the level of strain applied and the *strain rate* at which it was applied. Also, under multiple loads, the material becomes weaker and suffers some damage with each loading cycle or thermal stress application (Sutton and Biblarz, 2001). The mechanical properties are also function of the initial temperature of propellants.

1.1.9 Thermal Profile in a Burning Solid Propellant

It is highly beneficial to determine the thermal profile in the subsurface region of a steady-state burning solid propellant. This information can be utilized to determine the amount of thermal energy stored in the relatively thin layer under the burning surface and the energy transfer rate at the propellant surface. The burning rate of the propellant can also be related to the temperature distribution in the thermal wave as the burning surface regresses with time.

1.1.9.1 Surface and Subsurface Temperature Measurements of Solid Propellants

For a steady-state burning solid propellant with constant properties and no subsurface heat release, the energy equation—the heat conduction equation with a moving boundary at burning rate r_b —can be integrated with respect to the distance normal to the burning surface, y . The resulting integrated equation, given in terms of the dimensionless temperature and distance, has this form:

$$\theta \equiv \frac{T - T_i}{T_s - T_i} = \exp\left(-\frac{\dot{m}_p C_c y}{k_p}\right) = \exp\left(-\frac{\rho_p r_b C_c y}{k_p}\right) = \exp\left(-\frac{r_b y}{\alpha_p}\right) \quad (1.5)$$

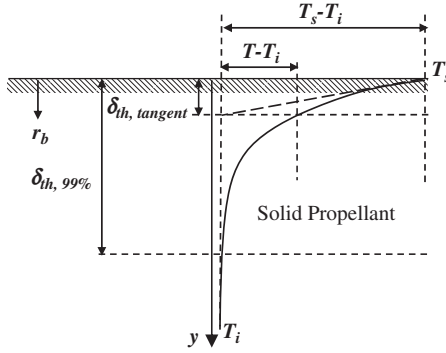


Figure 1.11 Thermal wave thicknesses in a burning solid propellant.

By differentiating Equation 1.5 with respect to y measured from the burning surface into the solid propellant (see Figure 1.11), we have

$$\frac{dT}{dy} = -\frac{(T_s - T_i)}{\alpha_p/r_b} \exp\left(-\frac{r_b y}{\alpha_p}\right) \quad \text{or} \quad \left.\frac{dT}{dy}\right|_{y=0} = -\frac{(T_s - T_i)}{\alpha_p/r_b}$$

The physical meaning of the term (α_p/r_b) represents a depth at which the tangent line to the temperature profile intersects with the initial temperature profile ($T = T_i = \text{constant}$). This thermal-wave thickness $\delta_{th, tangent}$ given in Equation 1.6 defined by the tangent line method is simply the ratio of the thermal diffusivity of solid propellant α_p to its burning rate r_b .

$$\delta_{th, tangent} = \frac{\alpha_p}{r_b} \quad \text{where} \quad \alpha_p \equiv \frac{k_p}{\rho_p C_c} \quad (1.6)$$

At this particular thermal wave depth, the dimensionless temperature $\theta = 0.368$. Although this is not the full thermal wave depth, it is referred in the solid propellant literature as the thermal wave depth, δ_{th} . Thermal wave thickness $\delta_{th, 99\%}$ also can be defined as the depth in the solid where $\theta = 0.01$. Usually,

$$d_{th, 99\%} = 4.605 d_{th, tangent} \quad (1.7)$$

The subsurface temperature profile of a burning propellant can be measured using a fine-wire thermocouple embedded in a propellant strand specimen. In order to achieve a lower measurement error, the thermocouple size must be much smaller than the thermal wave thickness. This means that the thermocouple bead size (or thickness) should be smaller than $0.2\alpha_p/r_b$, where α_p is the propellant thermal diffusivity and r_b the burning rate. For example, a typical propellant has $\alpha_p = 1.8 \times 10^{-3} \text{ cm}^2/\text{s}$. If $r_b = 1 \text{ cm/s}$, then $0.2\alpha_p/r_b = 3.6 \text{ }\mu\text{m}$, while $\delta_{th, 99\%} = 83 \text{ }\mu\text{m}$. The burning rate of solid propellant usually increases at higher pressures. As a result, the thermal wave thickness decreases. This presents a very stringent

requirement for the size of the thermocouple bead. Another important issue with the subsurface measurement is the consideration of heterogeneous nature of the composite propellant based on ammonium perchlorate (AP). Typical AP particle size ranges from 40 μm to 200 μm . The thermal wave penetration depth $\delta_{th,99\%}$ is of the same order as AP particle size. This implies that the heat transfer process in AP-composite propellants is essentially three-dimensional. The next example explained this case.

EXAMPLE 1.3

Evaluate the magnitude of $\delta_{th,99\%}$ of a typical AP-based composite propellant burning at the rate of 1 cm/s.

$$\left. \begin{array}{l} \rho_p = 1700 \text{ kg/m}^3 \\ C_c = 1465 \text{ J/kg-K} \\ k_p = 0.21 \text{ W/m-K} \end{array} \right\} \Rightarrow \alpha_p = 0.84 \times 10^{-3} \text{ cm}^2/\text{s} \left. \begin{array}{l} \\ \\ \\ r_b = 1 \text{ cm/s} \end{array} \right\} \Rightarrow \delta_{th,99\%} = 39 \mu\text{m}$$

Based on the observation from this example, the measurement of subsurface temperature in a propellant strand can be made only by extremely small thermocouples with sizes in the range of 1 to 2 μm . Some S-type thermocouple beads made of platinum (Pt) and Pt with 20% rhodium (Rh) wires can be rolled into a flat junction. For higher-temperature measurements, a D type of thermocouple made of tungsten (W) and rhenium (Re) can be used for measuring temperatures as high as 2,593 K.

The determination of the burning surface temperature is of great interest to the combustion community. From Equation 1.5, one can see that the temperature difference $T - T_i$ varies exponentially with the depth in the solid propellant. The temperature-time trace can be converted into temperature-distance plot. For propellants with an inert subsurface region, the temperature-distance plot can be given in form of a semi-log plot of T/T_i versus the distance y . On such a plot, the subsurface temperature profile should show a linear relationship in the solid-phase region, and the gas-phase temperature profile should show a departure from this straight line. Therefore, the location of the burning surface and the surface temperature can be determined from the departure point from the straight-line section.

1.1.9.2 Interfacial Energy Flux Balance at the Solid Propellant Surface

At the interface of solid propellant (or solid fuel) and gas-phase media, the energy flux balance can be written as (see Figure 1.12):

$$\underbrace{k_p \left[\frac{dT}{dx} \right]_{0^-}}_{\substack{\text{Heat flux into the} \\ \text{subsurface region} \\ \text{at } y = 0^- \text{ by conduction}}} = \underbrace{k_g \left[\frac{dT}{dx} \right]_{0^+}}_{\substack{\text{Heat flux from gas phase} \\ \text{to burning surface at } y = 0^+ \\ \text{by conduction}}} + \underbrace{\rho_p r_b Q_s}_{\substack{\text{Heat released at} \\ y = 0 \text{ due to chemical} \\ \text{reaction at surface}}} + \underbrace{I_f}_{\substack{\text{Heat feedback} \\ \text{from flame} \\ \text{zone to surface} \\ \text{by radiation or external} \\ \text{radiative energy source}}} \quad (1.8)$$

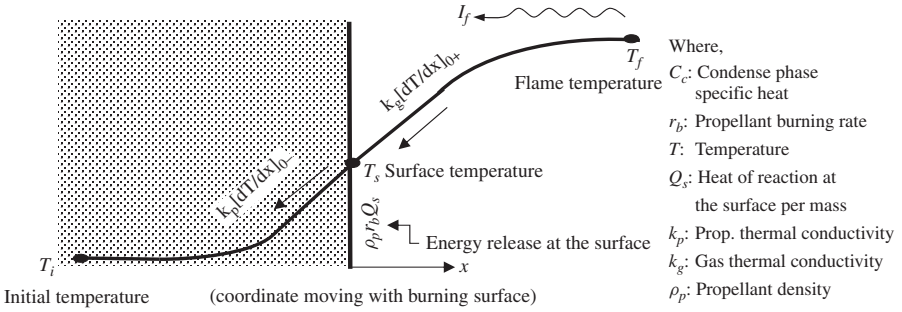


Figure 1.12 Energy flux balance at the interface between gas phase and solid phase.

where Q_s is the net heat release at the interface. The importance of the term I_f depends on the type of solid propellants and any external energy flux input by a laser beam or similar source. If there are no subsurface chemical reactions, then

$$k_p \left[\frac{dT}{dx} \right]_{0^-} = \rho_p r_b C_c (T_s - T_i) \tag{1.9}$$

Assuming that I_f is very small in the flux balance equation and utilizing the previous relationship, we have

$$k_g \left[\frac{dT}{dx} \right]_{0^+} = \rho_p r_b [C_c (T_s - T_i) - Q_s] \tag{1.10}$$

The slope change at the burning surface could vary depending on the magnitude of net energy release per unit surface area. If $\rho_p r_b Q_s$ term is high enough, the slope of temperature profile in the gas phase could be less steep.

As indicated from Figure 1.13, the thermal wave thickness is of the order of several hundred μm . As the pressure is increased, the temperature profile becomes steeper near the surface.

1.1.9.3 Energy Equation for the Gas Phase

In order to study the relationship between the propellant burning rate and the heat release processes in the gaseous flame, it is useful to consider the energy equation for the gas phase. If k_g and C_{pg} are independent of temperature, then the one-dimensional gas-phase energy equation can be written as:

$$k_g \frac{d^2 T}{dx^2} - \rho_g U_g C_{pg} \frac{dT}{dx} + \dot{\omega}_g^m Q_g = 0 \tag{1.11}$$

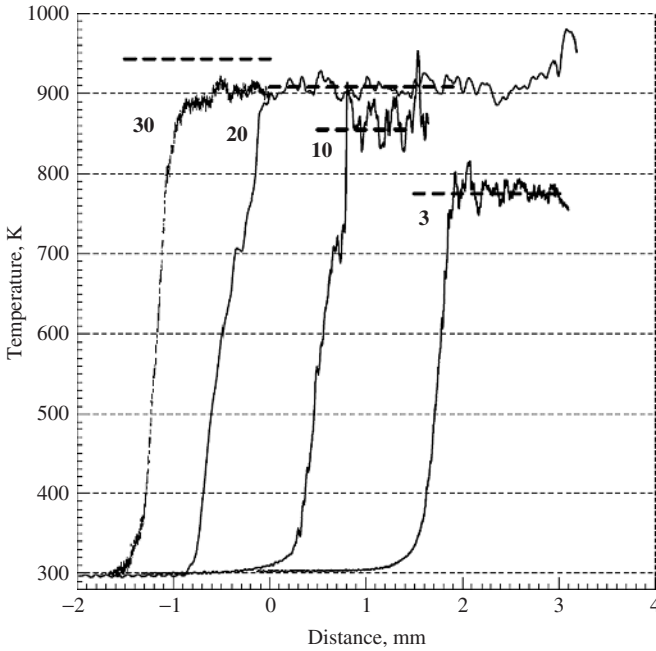


Figure 1.13 A set of recorded thermocouple traces for phase-stabilized AN (PSAN) with 4% $K_2Cr_2O_7$ at pressures 3, 10, 20, 30 MPa. Dashed lines are the dissociation temperatures of AN at corresponding pressures (modified from Sinditskii, et al., 2008).

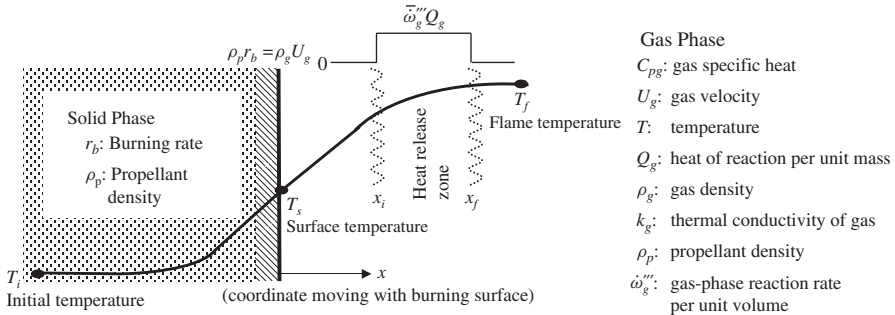


Figure 1.14 Assumed top-hat heat release profile in the gas-phase region.

Assuming that $\dot{\omega}_g''' Q_g$ is constant starting from x_i to x_f and zero elsewhere as shown in Figure 1.14, we can integrate Equation 1.11 to yield the next relationship:

$$k_g \left[\frac{dT}{dx} \right]_{0+} = Q_g \int_0^{\infty} \exp \left(-\frac{\rho_g U_g C_{pg}}{k_g} x \right) \dot{\omega}_g''' dx$$

$$\text{provided } \dot{\omega}_g''' Q_g = \begin{cases} 0 & 0 < x < x_i \\ \dot{\omega}_g''' Q_g & \text{for } x_i < x < x_f \\ 0 & x_f < x < \infty \end{cases} \quad (1.12)$$

At $x = x_i$, exothermic reaction starts; at $x = x_f$, heat release zone ends. By applying these conditions to Equation 1.12, we have:

$$k_g \left[\frac{dT}{dx} \right]_{0+} = \frac{k_g}{\rho_g U_g C_{pg}} \bar{\omega}_g''' Q_g \left\{ \exp \left(-\frac{\rho_g U_g C_{pg}}{k_g} x_i \right) - \exp \left(-\frac{\rho_g U_g C_{pg}}{k_g} x_f \right) \right\} \quad (1.13)$$

The reaction zone thickness is given as $\delta_{flame} = x_f - x_i$. If the reaction starts at the surface—that is, if $x_i = 0$ —then:

$$k_g \left[\frac{dT}{dx} \right]_{0+} = \frac{k_g}{\rho_g U_g C_{pg}} \bar{\omega}_g''' Q_g \left[1 - \exp \left(-\frac{\rho_g U_g C_{pg} x_f}{k_g} \right) \right] \quad (1.14)$$

$$\text{if } \left(\frac{\rho_g U_g C_{pg} x_f}{k_g} \gg 1 \right),$$

$$\text{then } k_g \left[\frac{dT}{dx} \right]_{0+} \cong \frac{k_g}{\rho_g U_g C_{pg}} \bar{\omega}_g''' Q_g \cong \frac{k_g}{\rho_p r_b C_{pg}} \bar{\omega}_g''' Q_g \quad (1.15)$$

For an extremely thin reaction zone located at $x = x_f$ (i.e., the flame-sheet case), reaction rate in the gas phase can be expressed by using mass continuity concept:

$$\int_0^{\infty} \dot{\omega}_g''' \delta(x - x_f) dx = \rho_g U_g = \rho_p r_b \quad (1.16)$$

where δ is the Dirac-delta function. Substituting the above relationship into the heat-flux balance in Equation 1.12 at $x = 0^+$, we get:

$$k_g \left[\frac{dT}{dx} \right]_{0+} = Q_g \int_0^{\infty} \exp \left(-\frac{\rho_g U_g C_{pg}}{\lambda_g} x \right) \dot{\omega}_g''' \delta(x - x_f) dx \quad (1.17)$$

or

$$k_g \left[\frac{dT}{dx} \right]_{0+} = \rho_g U_g Q_g \exp \left(-\frac{\rho_g U_g C_{pg}}{k_g} x_f \right) = \rho_p r_b Q_g \exp \left(-\frac{\rho_p r_b C_{pg}}{k_g} x_f \right) \quad (1.18)$$

1.1.9.4 Burning Rate of Solid Propellants

The burning rate of a propellant can be determined by using the interface heat-flux balance equation Equation 1.8 by assuming that the radiation flux I_f is relatively small, the surface heat flux of the solid propellant given by Equation 1.9, and the surface heat flux of the gas phase is Equation 1.15. One can obtain an explicit expression for the solid propellant burning rate. This expression is given by Equation 1.19.

$$r_b = \left[\frac{k_g \bar{\omega}_g''' Q_g}{\rho_p^2 C_{pg} [C_c (T_s - T_i) - Q_s]} \right]^{1/2} \propto (\bar{\omega}_g''' Q_g)^{1/2} \quad (1.19)$$

Generally, the reaction rate of a single-step forward reaction



can be written as:

$$\underbrace{\dot{\omega}'''_g}_{\substack{\text{Mass} \\ \text{generation} \\ \text{rate per} \\ \text{volume}}} = \underbrace{\left(\sum_{\text{products}} v''_i - \sum_{\text{reactants}} v'_i \right)}_{\substack{= \Delta n = \text{Difference} \\ \text{in stoichiometric} \\ \text{coefficients between} \\ \text{product and reactant species}}} \underbrace{k_f}_{\substack{\text{Reaction} \\ \text{rate} \\ \text{constant}}} \prod_{k=1}^N \underbrace{(\rho_g)^{v'_k}}_{\substack{\text{Gas} \\ \text{density}}} \underbrace{(X_k)^{v'_k}}_{\substack{\text{Mole} \\ \text{fraction}}} \quad (1.21)$$

Therefore, substituting this expression into Equation 1.19, we have:

$$r_b = \left[\frac{k_g Q_g \Delta n k_f \prod_{k=1}^N (\rho_g X_k)^{v'_k}}{\rho_p^2 C_{pg} [C_c (T_s - T_i) - Q_S]} \right]^{1/2} \quad (1.22)$$

Generally, the gas-phase reactions in the burning of energetic materials are bimolecular and of second-order (i.e., number of reactants [F and O] = 2 and $v'_F = v'_O = 1$); therefore:

$$r_b = \left[(k_g Q_g \Delta n k_f \rho_g^2 X_F X_O) / \left\{ \rho_p^2 C_{pg} [C_c (T_s - T_i) - Q_S] \right\} \right]^{1/2} \quad (1.23)$$

The reaction rate constant, k_f , is a function of gas temperature and is expressed in Arrhenius form as:

$$k_f = A_g \exp(-E_{a,g}/R_u T_g) \quad (1.24)$$

Under low-pressure conditions, the ideal gas law can be used to relate the gas density ρ_g with pressure p and gas temperature T_g by:

$$\rho_g = p / (RT_g) \quad (1.25)$$

Substituting Equations. 1.24 and 1.25 into Equation 1.22, we have:

$$r_b = p \left[\frac{k_g Q_g \Delta n X_F X_O A_g \exp(-E_{a,g}/R_u T_g)}{(RT_g)^2 \rho_p^2 C_{pg} [C_c (T_s - T_i) - Q_S]} \right]^{1/2} \quad (1.26)$$

Another way to express the burning rate of a solid propellant is by relating its burning surface temperature using the Arrhenius equation; that is

$$r_b = A_s T_s^\beta \exp(-E_{a,s}/R_u T_s) \quad (1.27)$$

The burning rate of a solid propellant is also given by the empirical Saint-Robert's law (or Vieille's law) as:

$$r_b = ap^n \quad (1.28)$$

where a usually is a function of the initial temperature T_i . This equation is valid only when the gas cross-flow velocity over the propellant surface is low enough so that shear-induced effects on the burning rate can be ignored. In the case of high-velocity flow of combustion gases over the burning propellant surface, a different equation must be used to include the erosive burning effect. For practical applications, a lower-pressure exponent is considered favorable since that implies relatively uniform burning of solid propellant during pressurization in the solid propellant rocket motor.

1.1.9.5 Temperature Sensitivity of Burning Rate

The burning rate of a solid propellant is dependent on pressure based on Equation 1.28. However, it is also dependent on the initial temperature of the propellant T_i , even when the pressure is kept constant. The parameter “ a ” in Equation 1.28 is not a true constant, since it can be expressed as a function of initial temperature T_i and temperature sensitivity σ_p . Hence,

$$a = a_{ref} e^{\sigma_p(T_i - T_{i,ref})} \quad (1.29)$$

The temperature sensitivity σ_p is defined as:

$$\sigma_p \equiv \frac{1}{r_b} \left[\frac{\partial r_b}{\partial T_i} \right]_P = \left. \frac{\partial \ln r_b}{\partial T_i} \right|_P \quad (1.30)$$

Using Equations 1.29 and 1.30, the burning rate can then be expressed as:

$$r_b = \left[a_{ref} e^{\sigma_p(T_i - T_{i,ref})} \right] p^n \quad (1.31)$$

The value of σ_p is often very small; therefore, the exponential term in Equation 1.31 can be linearized.

Numerous burning rate measurement methods have been developed by various researchers over many years of work in solid propellant combustion. A review of these methods has been given in a paper by Zarko and Kuo (1994). In general, there are two major categories for burning rate measurements: (1) standard *strand burners* method (also called Crawford burners), and (2) small-scale ballistic evaluation motors with known propellant web thickness. These two methods are described in the next subsections. In the second method, the motor firing is conducted and pressure-time traces are measured; along with the web thickness of the propellant, they are used to deduce the burning rate of the propellant.

1.1.9.6 *Measurement of Propellant Burning Rate by Using a Strand Burner*

A strand burner is a small pressure vessel (usually with windows) where a small propellant strand (e.g., diameter of usually ~ 6.5 mm and length ~ 50 – 100 mm) is installed to burn as an end-burning specimen for determining their burning rates under well-controlled P and T_i conditions by using an inert gas (e.g., nitrogen) to simulate pressurized conditions and different initial temperatures. All lateral surfaces are covered with inhibitor materials, leaving only the top surface exposed for burning.

The burning rate can be measured by electric signals from embedded wires, by optical means, or sometimes by ultrasonic waves. The most traditional method is to embed multiple break wires in the propellant strand at several locations along its length. Once the propellant is burned up to a length where the break wire is embedded, the wire breaks (hence its name) and stops sending the electric signal to the receiver. Similarly, the signal is stopped from the break wire at the next location along the propellant strand. The burning rate is determined by measuring the time needed to burn (the time between the two stopped signals) a fixed length of the propellant (the distance between two consecutive break wires inserted in the strand), and/or by visual measurements through a windowed burner. (see Figure 1.15.) The accuracy of regression rate measurements by this method depends on the error in the measurement of the sample length and the time of burning. Usually an inert gas, such as nitrogen, is used to pressurize the chamber and is allowed to flow continuously as purged gas during the test. The temperature of the purge gas can be controlled to desired levels for pre-conditioning the initial temperature of the strand. The burning rate measured by strand burners is usually lower than that obtained from full-scale solid propellant rocket motor firing (by 4%–12%) because it does not truly simulate hot chamber environments (see Sutton and Biblarz, 2001). The relationship between the burn rates measured by strand burner and motor firing usually is determined empirically for each propellant category and grain configuration. Strand burner data are useful in screening propellant formulations and in quality control operations. However, the data from the full-scale motors tested under a variety of conditions constitute the final proof of burning-rate behavior.

The burning surface condition of the propellant strand can vary significantly based on the ingredients used in the propellant formulation. A pure propellant ingredient, such as pressed RDX strand can generate a foam layer on its burning surface at a relatively low pressure, as shown in Figure 1.16a. In contrast, a homogeneous propellant called JA2 (containing mainly nitrocellulose, di-ethylene glycol-di-nitrate, and nitroglycerin) can generate many carbonaceous residues on the burning surface, as shown in Figure 1.16b. An RDX-based composite propellant called M43 (RDX/cellulose acetate butyrate or CAB/NC/plasticizers) can exhibit residuals on its surface and relatively nonuniform gaseous flame, as shown in Figure 1.16c. In spite of these multi-dimensional effects at the surface, the overall regression process still can be close to a one-dimensional process. For AP-based composite propellants, the AP crystals usually regress faster than

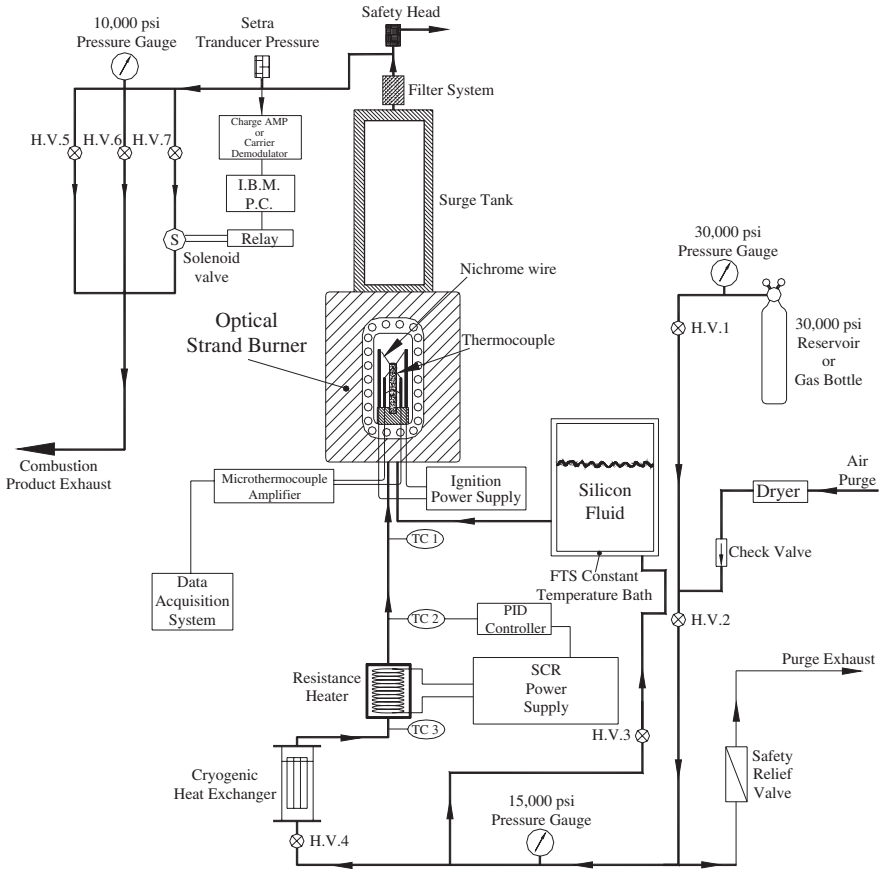
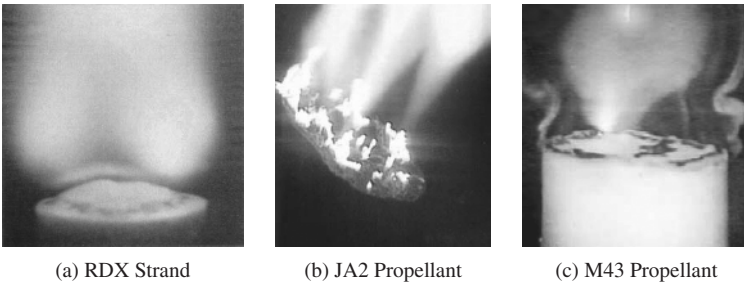


Figure 1.15 Schematic of a temperature- and pressure-controlled windowed strand burner.



(a) RDX Strand

(b) JA2 Propellant

(c) M43 Propellant

Figure 1.16 Close-up view of the surface burning behavior of three different propellants.

the fuel under high-pressure conditions, thereby making the surface nonflat, which introduces multidimensional effects.

1.1.9.6.1 Measured and Correlated Burning Rates of JA2 Propellant Combustion characteristics of JA2 propellant were studied both experimentally and theoretically by Kuo and Zhang (2006), who investigated the steady-state burning behavior was investigated by using an optical strand burner. The measured parameters were the regression rate, subsurface temperature profile, and burning surface temperatures at different initial temperatures ($-40 < T_i < 80^\circ\text{C}$) and pressures ($0.1 < p < 68 \text{ MPa}$). The measured burning rates were correlated with the initial temperature T_i and pressure up to 300 MPa, as shown in Figure 1.17.

As mentioned in Section 1.1.9.5, the burning rate is a function of pressure, initial temperature, and the temperature sensitivity Equation 1.31. The temperature sensitivity (σ_p) of JA2 was found to decrease as pressure increases, reaching an asymptotic value of 0.0024 K^{-1} at high pressures. Therefore, a correlation between the temperature sensitivity and pressure of the form shown in Equation 1.32 was proposed.

$$\sigma_p = \sigma_{p,c} + \frac{b}{c_1 + c_2 p} \quad (1.32)$$

Using the relation given in Equation 1.32 and Equation 1.31 with the measured data, the following parameter values were obtained from the burning-rate curve fitting procedure:

$$a_{ref} = 0.2478 \text{ (cm/s)(MPa)}^{-n}, \quad n = 0.8222, \quad \sigma_{p,c} = 0.00240 \text{ K}^{-1}, \\ b = 0.0537 \text{ K}^{-1}, \quad c_1 = 17.0425, \quad \text{and} \quad c_2 = 2.2108 \text{ MPa}^{-1}$$

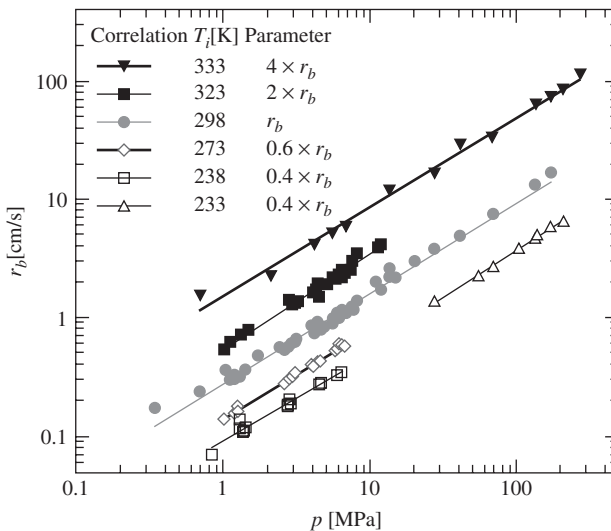


Figure 1.17 Measured burning rates of JA2 propellant at different initial temperatures as a function of pressure (Kuo and Zhang, 2006).

For a broad range of pressure, many propellants show a difference in the pressure exponent n (see Equation 1.28). This phenomenon is known as slope-break in burning rate expression, which represents the change in the burning mechanism of the solid propellant from one pressure regime to another. For JA2 propellant with ambient temperature as the initial temperature, its burning rate can be expressed by two different correlations. For a lower-pressure range $0.7 < p < 13.8$ MPa, r_b at $T_i = T_{amb}$ can be represented by Correlation A, as shown by Equation 1.33 and Figure 1.18.

$$r_b(\text{cm/s}) = 1.127[P(\text{MPa})/6.894]^{0.63} \quad (1.33)$$

For a higher pressure range $13.8 < p < 96.5$ MPa, at $T_i = T_{amb}$, r_b can be represented by Correlation B, as shown by Equation 1.34:

$$r_b(\text{cm/s}) = 5.822[P(\text{MPa})/48.26]^{0.97} \quad (1.34)$$

1.1.9.6.2 Burning Rate of Pressed Nitramine Ingredients In order to study the combustion behavior of solid propellants, it is helpful to understand the burning rate behavior of individual ingredients, even though such ingredients generally are not used as stand-alone propellants. For example, HMX and RDX are crystalline particles, and they are not used as monopropellants. However, pressed strands of HMX and RDX can be burned in a strand burner to obtain their respective burning rates and temperature sensitivities. Atwood et al. (1999) performed multiple measurements of the burning rates of these pressed nitramine ingredients

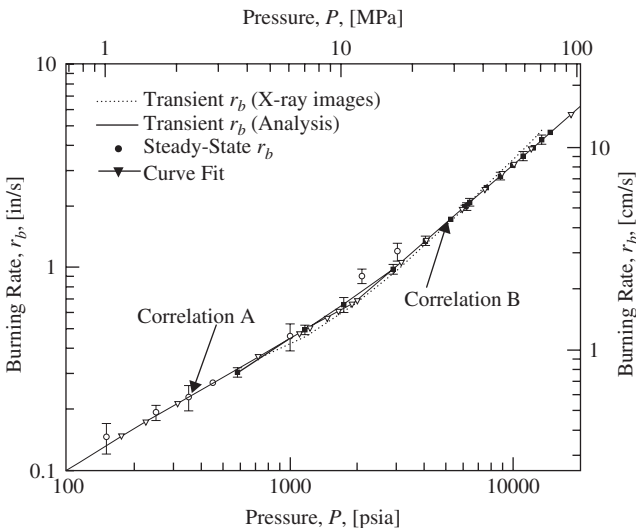
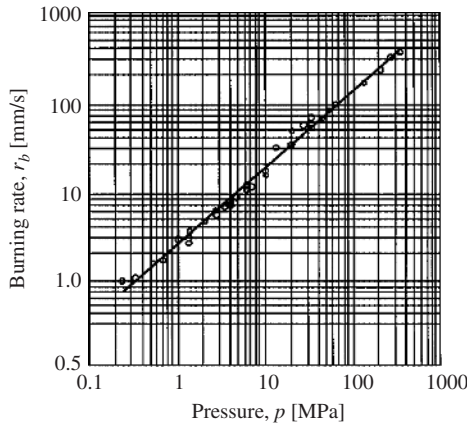
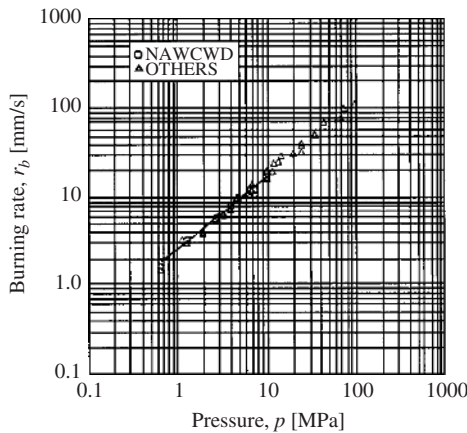


Figure 1.18 Measured burning rates of JA2 propellant at ambient temperatures as a function of pressure (Kuo and Zhang, 2006).



(a)



(b)

Figure 1.19 Measured burning rates of (a) β -HMX and (b) α -RDX at $T_i = T_{amb}$ (modified from Atwood et al., 1999a).

at various initial temperatures and pressures. At ambient temperatures, the burning rates of these two types of pressed strands are shown in Figure 1.19a and Figure 1.19b, respectively. The effects of initial temperature (T_i) on the burning rates of HMX and RDX are shown in Figure 1.20a and Figure 1.20b, respectively.

1.1.9.6.3 Burning Rate of Pressed Ammonium Perchlorate (AP) Strands Ammonium perchlorate (chemical formula: NH_4ClO_4) is an oxidizer and major ingredient in most composite solid propellants. Its behavior in the combustion zone greatly influences the overall combustion of the propellant. Therefore, an understanding of its deflagration behavior is an important step in understanding the complex combustion processes associated with the composite propellants. Pure AP has crystalline form (orthorhombic below 513 K and cubic above 513 K).

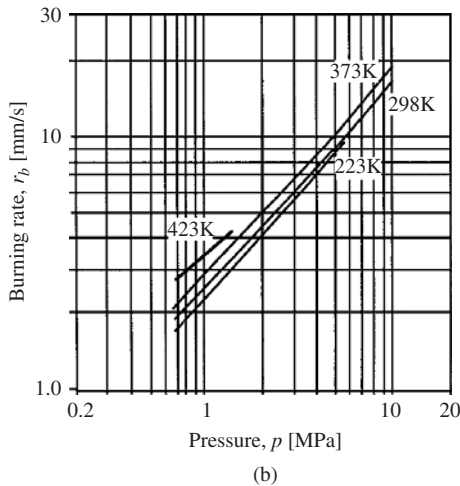
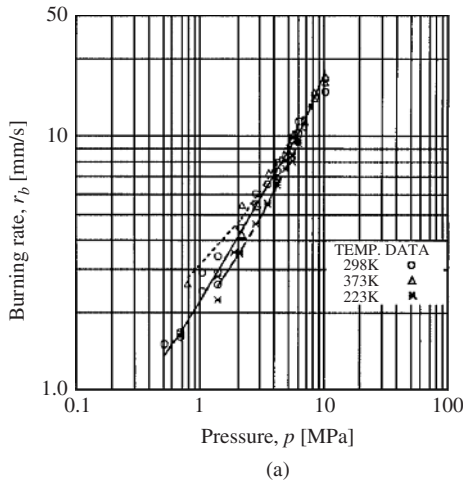


Figure 1.20 Effect of T_i on burning rates of pressed (a) β -HMX and (b) α -RDX strands (modified from Atwood et al., 1999b).

The burning rates of pressed AP strands (up to 335 MPa, with densities of 99.2%–99.4% of the theoretical maximum density [TMD]) have been measured by several researchers, including Boggs (1970) and Atwood et al. (1999a). These measurements were compared with similar data obtained by other researchers, as shown in Figure 1.21. The burning rate trend shows a dip in the pressure range between 13.8 and 27.6 MPa, which was attributed to unstable burning behavior reported by Boggs (1970) and *not* due to convective cooling. Above 27.6 MPa, the combustion process becomes more stable because of the dominance of gaseous species and gas-phase reactions. For this reason, the burning rate of AP again increases with pressure and shows a higher pressure exponent than the

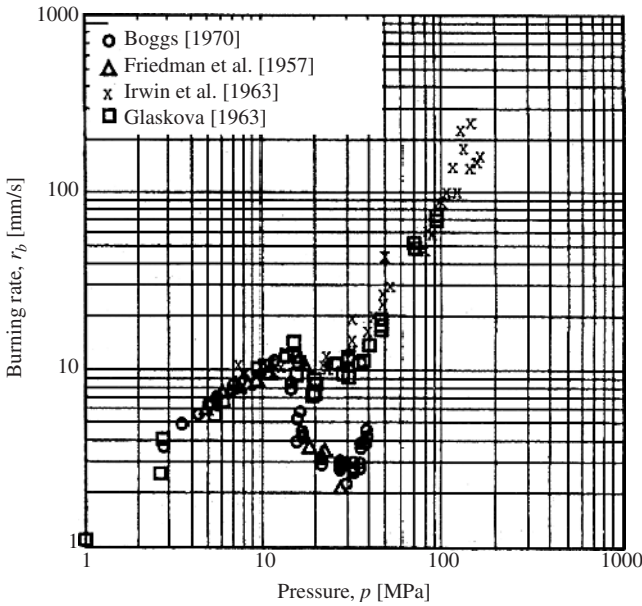


Figure 1.21 Measured burning rates of AP at $T_i = T_{amb}$ (modified from Atwood et al., 1999a).

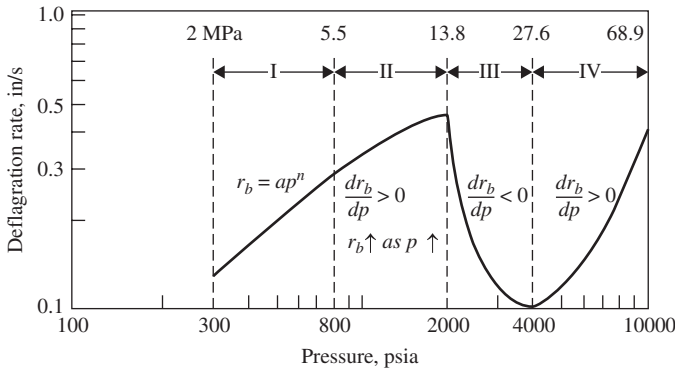

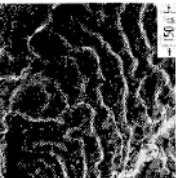
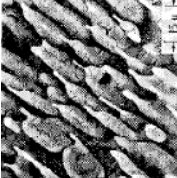
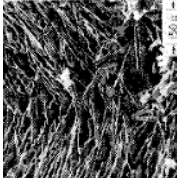


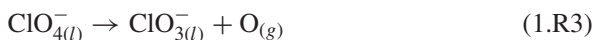
Figure 1.22 Measured burning rates of AP at $T_i = T_{amb}$ (modified from Boggs, 1970).

low-pressure regime. Figure 1.22 shows burning rate versus pressure curve with slope variations. Table 1.4 presents a detailed description of deflagration rate, surface structure, subsurface profile, and photographs of thermally quenched AP samples. The detailed analysis of unstable AP combustion mechanism is provided by Guirao and Williams (1971). Earlier, Boggs (1970) observed a liquid layer of AP on top of the solid AP crystals. The interphase reaction at the surface is likely to be the dissociative vaporization of liquid AP into NH_3 (g) and HClO_4 (g) from the liquid layer. This reaction is followed by the gas-phase combustion of

TABLE 1.4. Deflagration Rate, Surface Structure, and Subsurface Profile of Self-Deflagrating Single Crystals of Ammonium Perchlorate (modified from Boggs, 1970)

Re-gime	Pressure [MPa (psia)]	Rate [mm/s (in/s)]	Thermally quenched samples	Surface Characteristics	Subsurface Characteristics	Energy Transfer
I	2–5.5 (300–800)	3.3–7.6 (0.13–0.30)		Gas entrapped in liquid resulting in a froth. Thickness of liquid layer ↓ as p ↑,	Froth on cubic phase, cubic phase on orthorhombic phase	Exothermic froth
II	6.9–13.8 (1000–2000)	8.6–12.2 (0.34–0.48)		Ridges & valleys with activity sites in valleys, surface pattern spatially invariant with time	Ridges and valleys composed of cubic phase, activity sites extend depth of cubic phase	Condensed-phase and gas-phase coupled
III	13.8–27.6 (2000–4000)	12.2–2.54 (0.48–0.10)		Needles in areas of maximum regression	Thickness of layer of needles ~ 200–300 μm no needles at areas of minimum regression	Intermittent flame, local decomposition in needle array
IV	>27.6 (>4000)	>2.54 (>0.10)		Entirely covered in needles	Surface layer of needles on solid	Steady flame with uniform array of needles

AP not consumed in the liquid-phase reaction. The chain reaction mechanism is a multistage reaction in which the primary products are O_2 , H_2O , N_2O , NO , N_2 , HCl , and Cl_2 . The condensed-phase reaction is assumed to be a multistage reaction starting with the breakdown of the perchlorate ion:



At pressures above 15 MPa and below 30 MPa, the increased quantities of gas-phase species absorbed by the liquid layer inhibit the breakdown of perchlorate ion and cause a decrease in the burning rate (as observed by Atwood et al., 1999; Boggs, 1970; several other researchers). This in turn may lead to a decrease in surface temperature and extinction of the flame.

According to Guirao and Williams (1971), the deflagration mechanism at pressures above 30 MPa is qualitatively quite different from the mechanism between 15 and 30 MPa. At such high pressures, the thick ($>100 \mu\text{m}$) layer of “needles” may prevent the influence of observable gas-phase reactions (above the sample surface) on the regression rate. Processes occurring above the surface and within the needle forest (e.g., burning rates of needles) should govern the depth of the needle layer without appreciably influencing the regression rate. The regression rate may be determined by hidden processes occurring at the base of the needle layer, the surface of the virgin AP. It seems unlikely that this surface can be hot enough to support a sustained condensed-phase deflagration. Development of a finite-rate orthorhombic-to-cubic phase transformation, driven by heat from gas-phase reactions occurring at the base of the needle layer, may control the regression rate. In addition, crack propagation may also play a role in the regression mechanism.

The effect of initial temperature T_i on the burning rates of AP within a narrow pressure range (2–10 MPa) is shown in Figure 1.23. Even though the pressed AP cannot serve as a monopropellant, knowledge of its burning behavior is important as it is used broadly as a major oxidizer in many composite solid propellants.

1.1.9.6.4 Burning Rates of Six Monopropellants Hydrazinium nitroformate (HNF) with chemical formula of $N_2H_5^+C(NO_2)_3^-$ is an oxidizer with a very high energy content. The high energy density of HNF makes it an attractive candidate to replace oxidizers like AP that are currently in use for solid rocket propellants. According to Louwers (2000), HNF-based propellants could have up to 7% performance gain in comparison with existing AP-based solid propellants. Another advantage is that HNF-based solid propellants do not contain chlorine; therefore, the combustion products of these propellants are more environmentally benign. One of the major drawbacks of HNF is its nonspherical crystalline structure. Also, it is slightly hygroscopic, so special care must be taken during the processing and handling of HNF-based solid propellants. Earlier, it was also found that HNF was not compatible with the usual hydrocarbon binders, because HNF can attack the double bonds of unsaturated binders (Low, 1973). The potentially hazardous synthesis method of nitroform (one of the two main

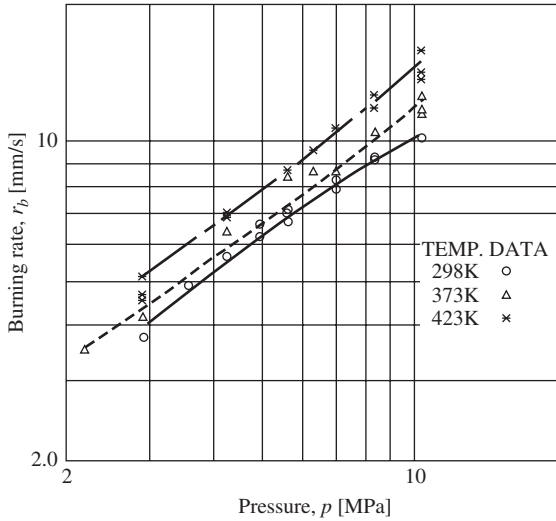


Figure 1.23 Effect of T_i on burning rates of neat pressed AP strands (modified from Atwood et al., 1999a).

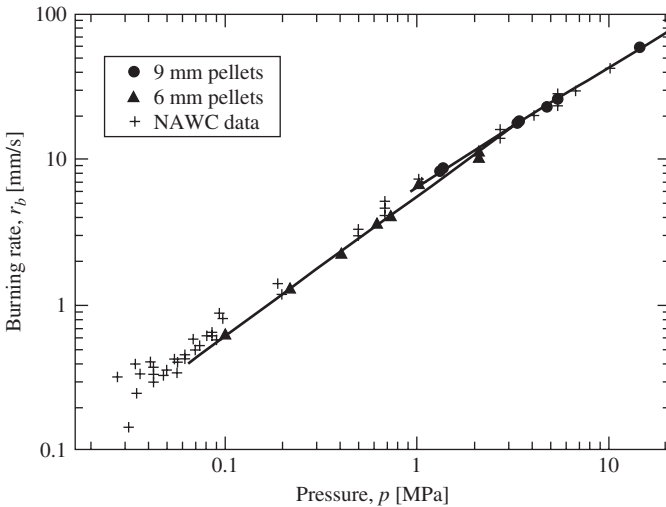


Figure 1.24 Burning rate of HNF monopropellant measured by Louwers (2000) and Finlinson and Atwood (NAWC, 1997). Note: The NAWC data below 0.2 MPa was obtained from short sample (2–3 mm only), which explains the increased scatter at these pressures (modified from Atwood et al. 1999a).

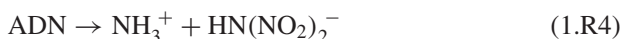
ingredients for HNF production) is also another concern. However, Louwers and van der Heijden (1999) discovered a technique to manufacture stable HTPB/HNF propellants. The measured burning rates of HNF monopropellant are shown in Figure 1.24. This plot shows three sets of burning rate data. The longer strands of HNF monopropellant (9 mm and 6 mm) were measured by Louwers (2000), and

the shorter strands (2–3 mm) were measured by Finlinson and Atwood (1997) at NAWC.

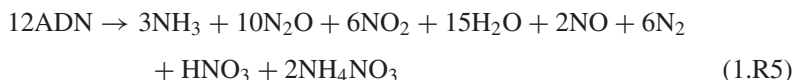
As shown in Figure 1.24, the neat HNF has a high burn rate pressure exponent ($n = 0.85–0.95$). At pressure below 2 MPa, the pressure exponent is 0.95; above 2 MPa, n is reduced to 0.85. At higher pressures, the samples were coated with a thin layer of Molycote 111 silicon grease to avoid flame spreading along the lateral surface of the sample. Due to its high pressure exponent, HNF is considered to be risky for practical applications in propulsion.

Ammonium dinitramide (ADN) is a new energetic material that can be used as an oxidizer in solid propellants. It is an ionic salt with the chemical formula $\text{NH}_4^+\text{N}(\text{NO}_2)_2^-$. This compound also presents an alternative to AP as it is an ecologically pure oxidizer in solid propellants. Although it was known and used in the Soviet Union in the 1970s (Agarwal and Hodgson, 2007), it did not gain attention on the world stage until after it had been synthesized by Bottaro et al. (1993a) in the late 1980s. ADN does not produce HCl in its combustion products and has a very attractive oxygen balance (+25.8%), although it has a slightly lower density than AP. Despite these qualities, ADN-based propellants have not been fully developed due to various shortcomings including high hygroscopicity, photosensitivity, and relatively low decomposition temperature ($\sim 135^\circ\text{C}$). Another major problem with ADN is the needlelike shape of its crystalline particles. A special prilling process is required to produce particles that have an improved shape for propellant processing and to reduce the hygroscopicity of the ADN (Doherty, 2008).

The thermal decomposition of ADN was studied by Brill et al. (1993) by using T-jump/FTIR spectroscopy with fast heating (2,000 K/s) of thin films on a platinum ribbon to a specified constant temperature between 220° and 300°C . Brill et al. proposed a reaction scheme consistent with their experimental observations and other experimental results, which was initiated by simple proton transfer:



At the onset of decomposition, gas evolution and sharp exothermicity occurred. The initial species observed were NH_3 , HNO_3 , and N_2O in comparable amounts and a small amount of NO_2 and ammonium nitrate (AN, chemical formula: NH_4NO_3). The scheme proceeded with decomposition of the dinitramidic acid $\text{HN}(\text{NO}_2)_2$, producing NO_2 and HNNO_2 , which then participated in subsequent reactions, resulting in this overall stoichiometric reaction:



The reaction 1.R5 produced significant amounts of NH_3 and NO_2 early in the decomposition process, which could then undergo further reaction according to the next overall reaction:



Brill et al. (1993) observed the formation of white smoke, which was attributed to the formation of AN aerosol from the recombination of NH_3 and HNO_3 in the cool atmosphere. It was postulated that AN aerosol would not be formed if a flame were present because NH_3 and HNO_3 would then react before recombining. The product ratios of detected species were $12\text{N}_2\text{O}:6\text{NO}_2:3\text{AN}:2\text{NH}_3:\text{HNO}_3:\text{NO}$ after the decomposition of ADN was completed. It is believed that ADN will be considered in the future energetic propellant development, especially for green propulsion.

Another high-energy crystalline oxidizer is known as CL-20 (also called HNIW). It was developed by Nielson at NAWC-China Lake (1988). Its official name is hexanitrohexaazaisowurtzitane, and its chemical formula is $\text{C}_6\text{H}_6\text{N}_{12}\text{O}_{12}$. The CL-20 molecule is a caged compound, and it exhibits polymorphism with five different polymorphic forms. The polymorph with the highest density is the ϵ -CL-20; therefore, it is the most desirable from a detonation pressure standpoint. The molecular structure of the CL-20 is shown in Figure 1.25.

The oxygen balance of ϵ -CL-20 is -11% , which is higher than that of RDX and β -HMX at -21.6% . The heat of formation of CL-20 is also greater than that of RDX and β -HMX. Since CL-20 is a higher-energy compound, it is more sensitive to shock than RDX and β -HMX. It is a potential candidate ingredient to be incorporated into advanced propellants (often considered very expensive) and explosives in the future. Figure 1.26 compares the measured burning rates of these neat propellants. It can be observed that ADN, HNF, and CL-20 show higher burning rates than RDX, HMX, and AP. The nitramines RDX and HMX have comparable burning rates, but their rates are only half the burning rates of CL-20. HNF shows highest burning rate exponent among all neat ingredients, significantly greater than that of ADN, as shown in Figures 1.26 and 1.27. A similar plot with comparison of burning rates of ADN and AP is shown in Figure 1.28. It is important to note that a lower-pressure exponent is preferred for rocket propellant formulation. Therefore, the burning rate of ADN makes it very attractive for future propellant development.

1.1.9.7 Measurement of Propellant Burning Rate by Using a Small-Scale Motor

“Web thickness” (L_w) can be defined as the minimum thickness of the grain from the initial burning surface to the insulated case wall of the motor or to the intersection of another burning surface. For example, for an end-burning grain,

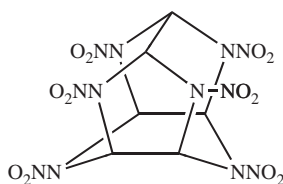


Figure 1.25 Molecular structure of CL-20 (Nielson, 1988).

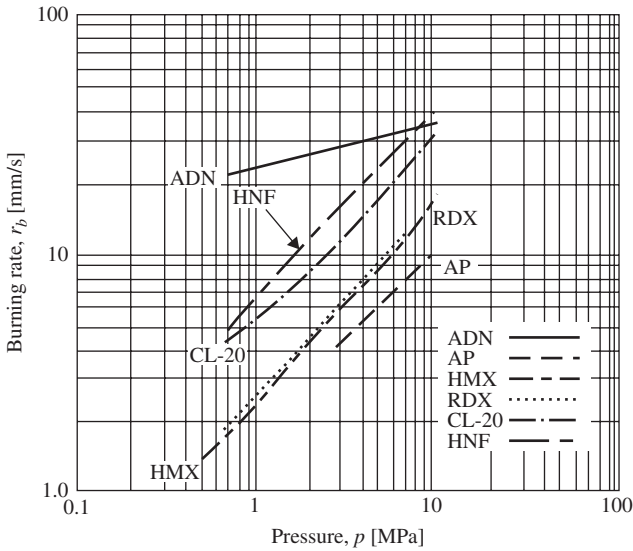


Figure 1.26 Comparison of burning rates of six different monopropellants at $T_i = T_{amb}$ (modified from Atwood et al., 1999a).

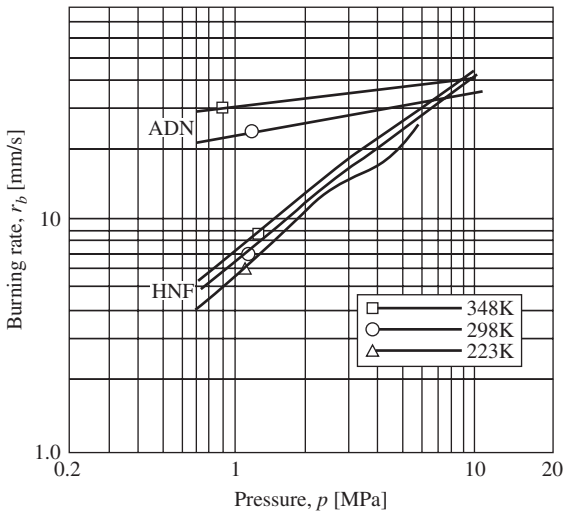


Figure 1.27 Comparison of burning rates of ADN and HNF at different p and T_i (modified from Atwood et al., 1999a).

the web thickness is the length of the propellant grain. For a center perforated grain, as shown in Figure 1.29, the web thickness is the difference between outer and inner diameters of the solid propellant grain. Note that the ballistic evaluation motor with the center perforated grain is the standard motor for burn rate determination.

“Web burnout duration” (t_b) can be defined as the duration from the propellant surface ignition time to the web burnout time on the measured pressure-time trace.

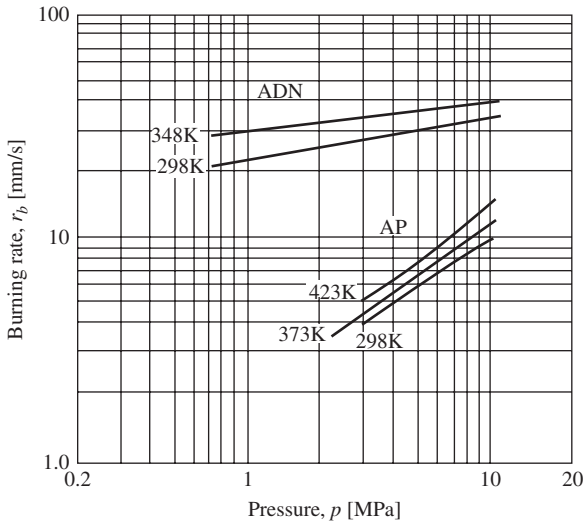


Figure 1.28 Comparison of burning rates of ADN and AP at different p and T_i (modified from Atwood et al., 1999a).

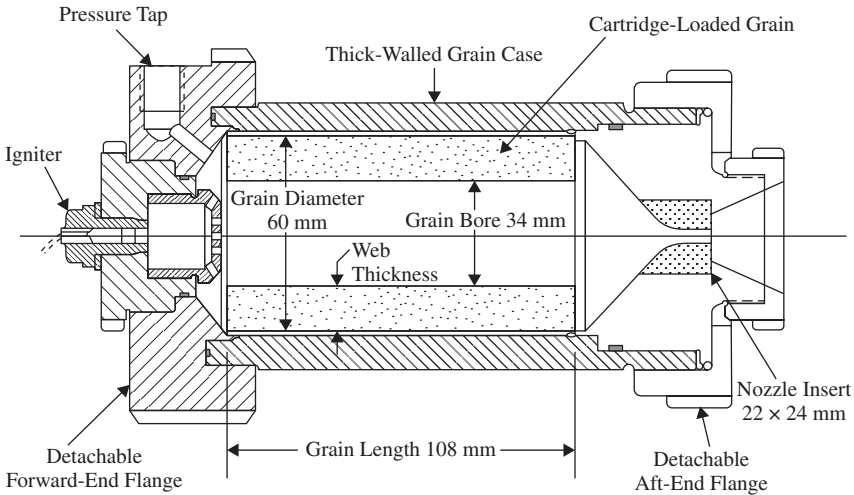


Figure 1.29 A typical small-scale ballistic evaluation motor (modified from Fry, 1998).

(see Figure 1.30.) Several techniques are used, and none has proven superior in all applications. The surface ignition time has been identified with various points on the primary rise portion of the trace:

1. The inverse tangent bisector (point t_A)
2. A fixed pressure or a fixed percentage of the average or maximum pressure (point t_B)
3. The initial inflection (point t_C)
4. The tangent-bisector (point t_D)

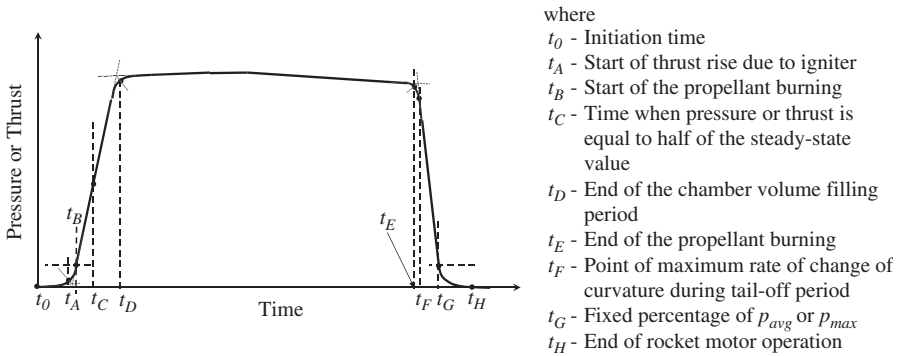


Figure 1.30 Definition of various times associated with a typical pressure-time trace of a motor firing (modified from Miller and Barrington, 1970).

Web burnout time has been identified with:

1. The aft tangent-bisector (point t_E)
2. The point of maximum rate of change of curvature during tail-off (point t_F)
3. A fixed pressure or fixed percentage of the average or maximum pressure (point t_G)

There are two major methods for characterizing burning rate of solid propellants in rocket motors. Hessler and Glick (2000), among other researchers, have discussed these two methods; one is based on the total web thickness over the burning time (TOT), and the second one is based on the mass balance (MB) on the motor firing results.

The fundamental TOT (thickness over time) burning rate may be defined:

$$r_{b,TOT} = \frac{L_{w,B} - L_{w,E}}{t_E - t_B} = \frac{\text{web thickness burned}}{\text{burning time}} \quad (1.35)$$

The mass balance (MB) burning rate is more complex and is defined as:

$$r_{b,MB} = \underbrace{\frac{L_{w,A} - L_{w,G}}{t_E - t_B}}_{\text{First equality}} \underbrace{\frac{\int_{t_B}^{t_E} p dt}{\int_{t_A}^{t_G} p dt}}_{\text{Second equality}} = \frac{\text{web thickness}}{\text{burning time}} \times \alpha_m \quad (1.36)$$

In Equation 1.36, α_m is the correction factor, and the storage in the rocket motor was ignored. The web thickness in the first equality of the equation is by derivation of total web thickness burned defined by the endpoints t_A and t_G during the total motor operating time defined by the endpoints t_E and t_B ;

however, it is almost universal practice to use the web thickness as indicated by the second equality. Although the original derivation of this equation is not known, redevelopment (Hessler and Glick 1998, and Glick, 1975) indicates that this apparent inconsistency is exactly offset by what appears to be an error in the assumptions necessary for the derivation. Both of these methods yield some errors from the full-scale motor testing. An evaluation of these two methods is provided in a report by Fry et al. (2002). For the comparison and error analysis of various burning rate measurement procedures, readers are referred to the paper by Hessler and Glick (2000).

1.1.9.8 Burning Rate Temperature Sensitivity of Neat Ingredients

The temperature sensitivity σ_p of the propellant burning rate is a function of chemical composition of propellants. The mathematical form of σ_p is given in Equation 1.30. The temperature sensitivity of the propellant burning rate of most energetic materials is not a constant parameter but usually depends on pressure. Burning rate temperature sensitivity should be made over a large enough pressure range to ascertain the effects of both pressure and initial temperature. The experimental data should be examined for consistency. It should be noted that extrapolation usually does not yield good results. Burn-rate temperature sensitivity of a propellant must be measured over evenly spaced temperature intervals that cover a range below and above ambient temperature to achieve more reliable data. A single parametric value for σ_p does not adequately describe the complexities of the combustion process. Therefore, the temperature sensitivity is generally given as a data set over a pressure range.

The burning rates of AP shown in Figure 1.26 are presented in a different format using the initial temperature at the abscissa as shown in Figure 1.31.

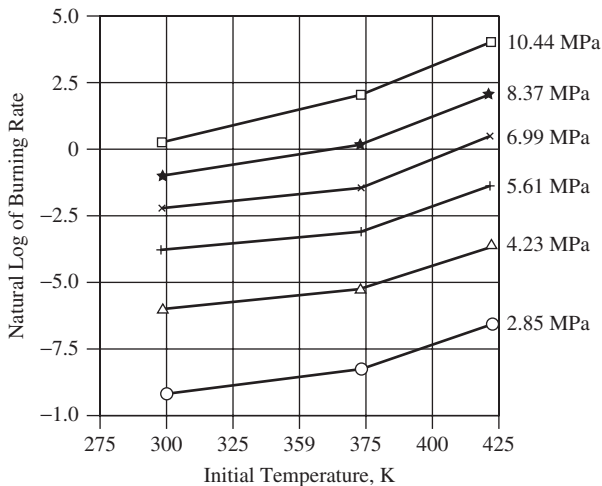


Figure 1.31 Natural log of AP burning rate versus initial temperature at different p (modified from Atwood et al., 1999b).

As shown in this plot, the difference in burning rates between two adjacent isobars decreases as the pressure increases. This fact indicates that the burning rate temperature sensitivity is a function of pressure and decreases with pressure. Using the cubic spline fit of the isobaric curves, the temperature sensitivities of AP can be deduced and compared with that of ADN in Figure 1.32. Similar comparisons are shown in Figure 1.33 for RDX, HMX, and CL-20 and in Figure 1.34 for ADN and HNF.

In general, the propellant ingredients with low temperature sensitivities are preferred as they have more consistent performance under different operating

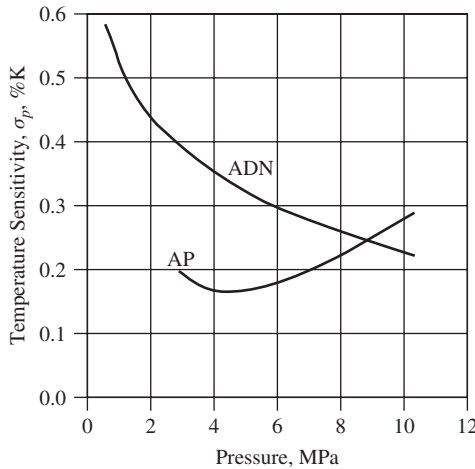


Figure 1.32 Combined plot of the burning rate sensitivities of ADN and AP (modified from Atwood et al., 1999b).

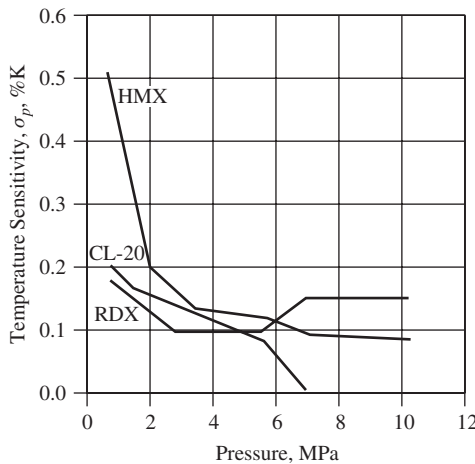


Figure 1.33 Combined plot of the burning rate sensitivities of HMX, RDX, and CL-20 (modified from Atwood et al., 1999b).

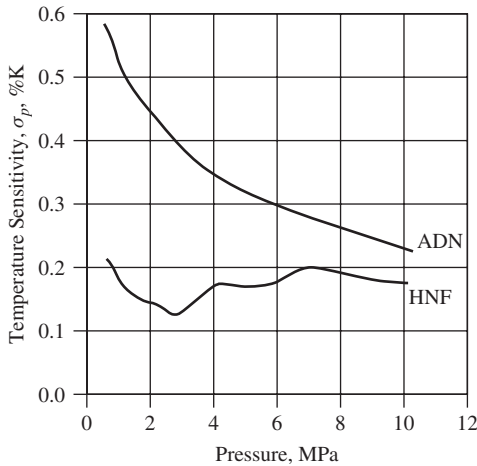


Figure 1.34 Combined plot of the burning rate sensitivities of ADN and HNF (modified from Atwood et al., 1999b).

conditions. It should be noted that a single parametric value for temperature sensitivity does not adequately describe the complexities of the burning rate dependency on initial temperature. Usually, σ_p is a function of pressure, as shown in Equation 1.33 for JA2 by Kuo and Zhang (2006).

1.2 SOLID-PROPELLANT ROCKET AND GUN PERFORMANCE PARAMETERS

A major application of solid propellants is in rocket and gun propulsion systems. This section provides definitions of the performance parameters for solid-propellant rocket motors and gun propulsion systems. The important parameters for rocket motors are specific impulse, characteristic velocity, thrust coefficient, density impulse, pressure sensitivity parameter, and thrust-coefficient efficiency. The significant performance parameters for solid-propellant gun systems include: muzzle velocity, pressure-travel curve, maximum pressure, velocity-travel curves, piezometric efficiency, ballistic efficiency, gun-propellant impetus, thermal efficiency, characteristic coefficient, relative quickness, relative force, and dynamic vivacity. Many of these parameters are generally considered for the formulation and development of modern solid propellants for both rocket and gun propulsion systems. The relationship between propellant burning rate behavior and these performance parameters is of critical importance and is discussed in this section. Burning solid propellants produce high-temperature combustion products that can be expanded through a converging-diverging nozzle to generate thrust for rocket propulsion. Although the propellant grains can have many different cross-sectional shapes, as given by Sutton and Biblarz (2010), generally two types of

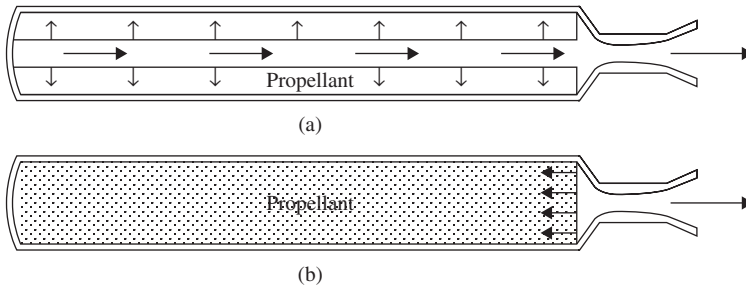


Figure 1.35 Two types of solid-burning rocket motors: (a) side burning and (b) end burning (modified from Kubota, 2007).

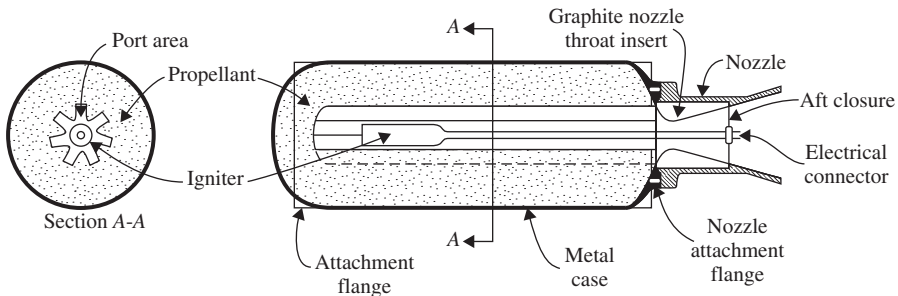


Figure 1.36 A side-burning solid propellant grain with the star-shaped cross section (modified from Sutton, 1992).

solid propellant grains are used in rockets: side-burning grain and end-burning grains (see Figure 1.35).

The side-burning propellant grain could have a star-shaped port with propellant bonded to the rocket motor case, as shown in Figure 1.36. In this design, the igniter is initiated in the cavity region toward the fore-end of the motor, and the energy for the ignition is supplied through an electrical connector mounted on the aft-end closure.

1.2.1 Performance Parameters of a Solid Rocket Motor

1.2.1.1 Thrust of a Solid Rocket Motor

Thrust is a result of pressure force distribution over interior and exterior surfaces of the motor. The net force acting on the interior surfaces of the solid rocket motor can be designated as F_i , which is equal to the sum of the total axial momentum of the exhausting jet and the pressure force acting on the exit plane. The total axial momentum of the exhausting jet is equal to the product of propellant mass burning rate (\dot{m}_p) and the average exhaust jet velocity (V_e). In steady state, this can be written as:

$$F_i = \dot{m}_p V_e + p_e A_e \quad (1.37)$$

The interior force acting on the combustion products has an equal and opposite reaction force, which acts on the rocket interior walls. This reaction force is the main driving force for the thrust generation. The net pressure force acting on the exterior surfaces of the rocket motor is due to the ambient pressure. The instantaneous thrust (F) can be evaluated from the difference between the reaction interior force and the net pressure force acting on the exterior surfaces of the rocket motor; that is,

$$F = F_i - F_e = \dot{m}_p V_e + A_e (p_e - p_{amb}) \quad (1.38)$$

The thrust also can be expressed as the product of a dimensionless thrust coefficient C_F , the nozzle throat area A_t , and average chamber pressure p_c , as shown next.

$$F = C_F A_t p_c \quad (1.39)$$

Consider that the nozzle exit station has a divergence angle α_d measured from the axis of the nozzle. This means that not all the jet momentum is in the axial direction. Therefore, a new parameter λ should be introduced to account for the loss of axial momentum in the thrust calculations. The λ parameter can be evaluated by the next equation:

$$\lambda = \frac{1 + \cos\alpha_d}{2} \quad (1.40)$$

With this correction, the thrust of a rocket motor can be evaluation from:

$$F = \lambda \dot{m}_p V_e + A_e (p_e - p_{amb}) \quad (1.41)$$

From the isentropic flow relationships, the average flow velocity at the nozzle exit plane (V_e) can be determined from the next equation:

$$V_e = \sqrt{\frac{2\gamma}{(\gamma - 1)} RT_c \left[1 - \left(\frac{p_e}{p_c} \right)^{\frac{\gamma-1}{\gamma}} \right]} \quad (1.42)$$

where

- T_c and p_c = temperature and pressure of the combustion product gases in the rocket motor combustion chamber, respectively
- R and γ = gas constant and specific heat ratio of the combustion product gases

It should be noted that the combustion products of nonmetallized solid propellants usually consist of gaseous products only. If the solid propellant contains metal particles, such as aluminum, then the combustion products of such

propellants will have significant amount of condensed-phase products, such as aluminum oxide. Under steady-state operation, the gaseous mass generation rate from burning a nonmetallized solid propellant is equal to the mass discharge rate through a choked nozzle. Therefore, the choked flow equation can be used to determine the mass flow rate of the gaseous combustion products through the nozzle:

$$\dot{m}_g = \Gamma(\gamma) \frac{p_c A_t}{\sqrt{RT_c}} = \Gamma(\gamma) p_c A_t \sqrt{\frac{M_w}{R_u T_c}} \quad (1.43)$$

In Equation 1.43, Γ is defined as:

$$\Gamma(\gamma) = \sqrt{\gamma} \left(\frac{2}{\gamma + 1} \right)^{\frac{\gamma+1}{2(\gamma-1)}} \quad (1.44)$$

Using Equations 1.40, 1.42, and 1.43 and continuing with Equation 1.41, we can obtain the next expression for the thrust:

$$F = p_c A_t \left\{ \lambda \Gamma \sqrt{\frac{2\gamma}{\gamma-1} \left[1 - \left(\frac{p_e}{p_c} \right)^{\frac{\gamma-1}{\gamma}} \right]} + \frac{A_e}{A_t} \left(\frac{p_e}{p_c} - \frac{p_{amb}}{p_c} \right) \right\} \quad (1.45)$$

A comparison of Equation 1.39 with Equation 1.45 yields this expression for the thrust coefficient C_F :

$$\begin{aligned} C_F &= \lambda \Gamma \underbrace{\sqrt{\frac{2\gamma}{\gamma-1} \left[1 - \left(\frac{p_e}{p_c} \right)^{\frac{\gamma-1}{\gamma}} \right]}}_{C_{F0}} + \frac{A_e}{A_t} \left(\frac{p_e}{p_c} - \frac{p_{amb}}{p_c} \right) \\ &= \lambda C_{F0} + \frac{A_e}{A_t} \left(\frac{p_e}{p_c} - \frac{p_{amb}}{p_c} \right) \end{aligned} \quad (1.46)$$

From the plot of C_F versus A_e/A_t shown in Figure 1.37, it can be easily seen that it is desirable to have the combustion products expanded to the ambient pressure for reaching maximum C_F . Under optimum expansion conditions, the exhaust pressure p_e should be equal to the ambient pressure p_{amb} as shown in Figure 1.38. Also note that optimum expansion cannot be achieved during a flight of a rocket with altitude variations, since the ambient pressure changes accordingly. Figure 1.39 shows the effect of pressure expansion ratio on the C_F at optimum expansion.

During transient burning conditions, the mass generation rate by burning of the nonmetallized solid propellant can be different from the mass discharge rate through the nozzle. This results in change in the gaseous mass in the rocket motor

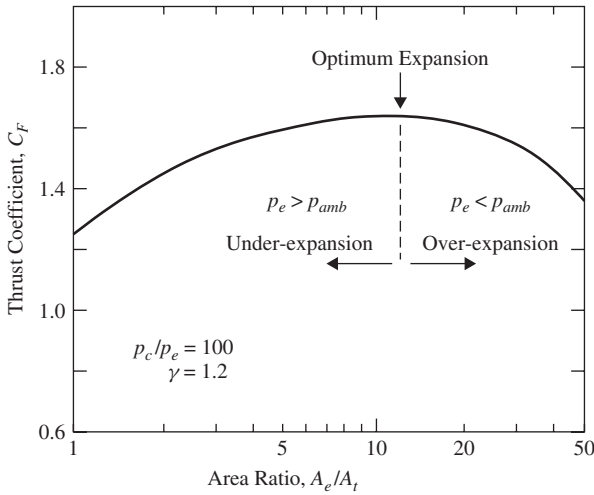


Figure 1.37 Variation of thrust coefficient with area expansion ratio (modified from Kubota, 1984).

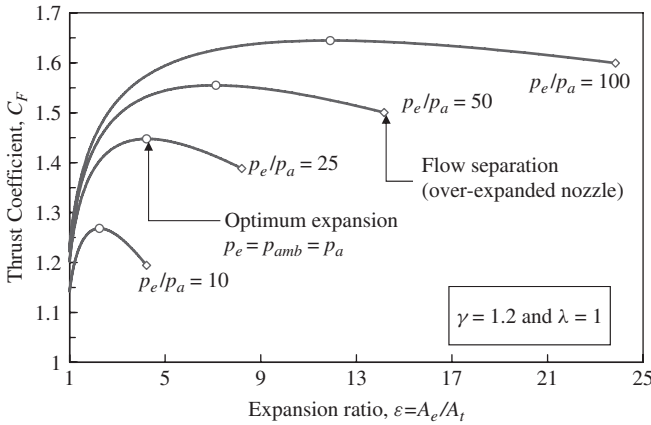


Figure 1.38 Variation of thrust coefficient with area expansion ratio at several specified pressure ratios. (The maximum on each curve represents the optimum expansion condition).

combustion chamber. Considering the entire rocket motor as a control volume, the mass balance in the rocket motor can be written as:

$$\frac{dm_{cv}}{dt} = \frac{d(\rho_g V_{cv})}{dt} = \dot{m}_g - \dot{m}_d \tag{1.47}$$

The mass generation rate by burning of the nonmetalized solid propellant can be expressed as:

$$\dot{m}_g = \dot{m}_p = \rho_p A_b r_b \tag{1.48}$$

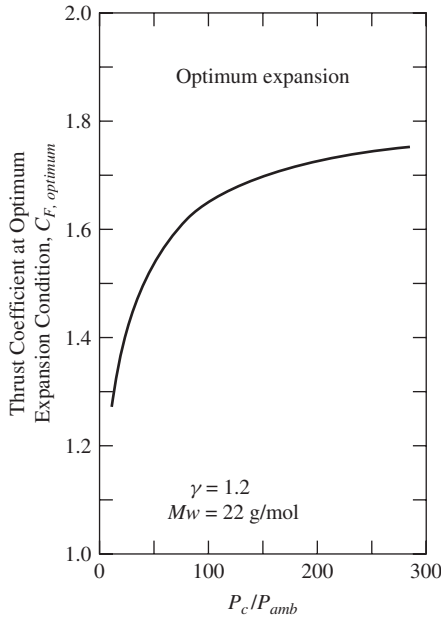


Figure 1.39 Variation of thrust coefficient at optimum expansion with pressure ratio (modified from Kubota, 1984).

The rate of mass discharge through the nozzle can be expressed as:

$$\dot{m}_d = C_D A_t p_c \quad (1.49)$$

The mass flow factor C_D in Equation 1.49 is defined as

$$C_D \equiv \frac{\Gamma(\gamma)}{\sqrt{RT_c}} = \sqrt{\gamma \left(\frac{2}{\gamma+1} \right)^{\frac{\gamma+1}{\gamma-1}} \frac{M_w}{R_u T_c}} \quad \text{Unit of } C_D : \left[\frac{\text{time}}{\text{length}} \right] \quad (1.50)$$

It is important to note that the parameter C_D should not be confused with the dimensionless flow discharge coefficient, which is usually expressed as C_d .

For steady-state burning conditions, the mass balance equation Equation 1.47 can be written as $\dot{m}_g = \dot{m}_d$. By utilizing Equations 1.39 and 1.49, we find:

$$\rho_p A_b r_b = C_D A_t p_c = \frac{C_D}{C_F} F \quad (1.51)$$

1.2.1.2 Specific Impulse of a Solid Rocket Motor

Total impulse is the thrust force integrating over burning time:

$$I_t \equiv \int_{t_0}^{t_E} F dt \quad \text{Units: (N-s)} \quad (1.52)$$

The specific impulse is defined as the total impulse per unit weight of propellant burned:

$$I_{sp} \equiv \frac{\int_{t_0}^{t_E} F dt}{g_0 \int_{t_0}^{t_E} \dot{m}_g dt} = \frac{I_t}{M_p g_0} = \frac{I_t}{W_p} \tag{1.53}$$

where g_0 ($=9.8066 \text{ m/s}^2$) is the gravitational acceleration at sea level and W_p is the weight of the propellant at sea level. Note that the thrust level of a rocket usually is a function of time. For special cases, we can have constant thrust level for majority of motor operation time as shown in Figure 1.30.

In the general case of static firing of the solid rocket motor with time varying thrust, the average thrust can be defined as:

$$F_{avg} = \frac{1}{t_E - t_C} \int_{t_C}^{t_E} F dt \tag{1.54}$$

Similarly, the average pressure is defined as:

$$p_{avg} = \frac{1}{t_E - t_C} \int_{t_C}^{t_E} p dt \tag{1.55}$$

In the case of a constant thrust operation, the specific impulse can be simplified as:

$$I_{sp} \cong \frac{F}{\dot{m}_p g_0} \tag{1.56}$$

From Equation 1.51, the thrust can be written as:

$$F = \frac{C_F}{C_D} \dot{m}_p \tag{1.57}$$

Substituting Equation 1.57 in Equation 1.56, we have:

$$I_{sp} = \frac{C_F}{C_D g_0} \tag{1.58}$$

Substituting C_D in Equation 1.58, we have:

$$I_{sp} = \frac{C_F/g_0}{\sqrt{\gamma \left(\frac{2}{\gamma+1}\right)^{\frac{\gamma+1}{\gamma-1}} \frac{1}{R_u}}} \sqrt{\frac{T_c}{Mw}} \quad \text{or} \quad I_{sp} \propto \sqrt{\frac{T_c}{Mw}} \tag{1.59}$$

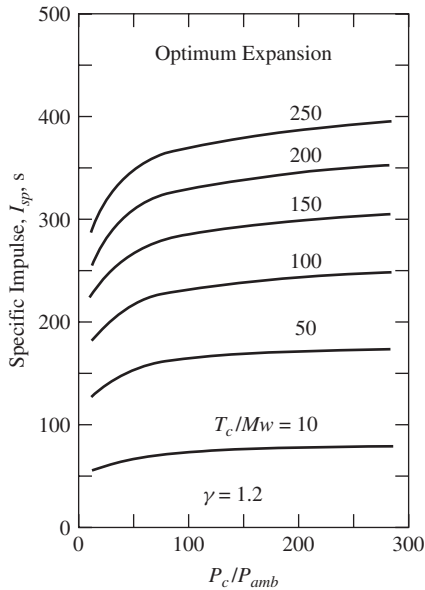


Figure 1.40 Dependency of I_{sp} on T_c/M_w (modified from Kubota, 1984).

From this relationship, it can be seen that the propellants with higher flame temperature (which dictates the chamber temperature, T_c) and lower molecular weight combustion products are desirable for producing high I_{sp} . The effect of T_c/M_w on the I_{sp} is shown in Figure 1.40 under optimum expansion condition. The effect of p_c/p_e can also be observed from this plot. It can be seen that T_c/M_w has a stronger effect on I_{sp} than p_c/p_e ; however, it is still very important to consider the possibility of increasing C_F by operating rocket motors at higher pressures (see Figure 1.39).

For a double base (DB) propellant, the flame temperature T_f and the specific impulse I_{sp} is affected by the concentration of nitroglycerine (NG), as shown in Figure 1.41.

Figure 1.42 shows the T_f and I_{sp} variations with the concentration of AP and RDX expressed in weight percent for the AP-based composite modified double-base (CMDB) propellants and RDX-based CMDB propellants. Although the scale on the AP and RDX weight percentages extends from 0 to 100 wt%, it is not practical to increase the solid loading of propellants beyond 88 wt%. Solid RDX without any binder material (also known as neat RDX) cannot be used as a propellant, although neat RDX can be used as an explosive material. For a specific CMDB propellant using AP as a filler material, the performance reached the peak around 50 wt% loading of AP particles. The AP-CMDB shows a decrease in T_f and I_{sp} when the AP weight percentage is above 50 wt% from the thermochemical calculations. The thermochemical properties

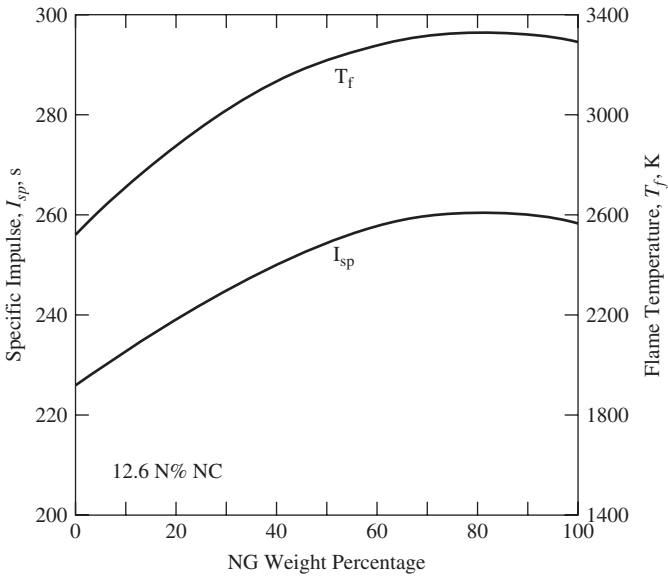


Figure 1.41 Variation of flame temperature and specific impulse with NG concentration of a double-base propellant (modified from Kubota, 1984).

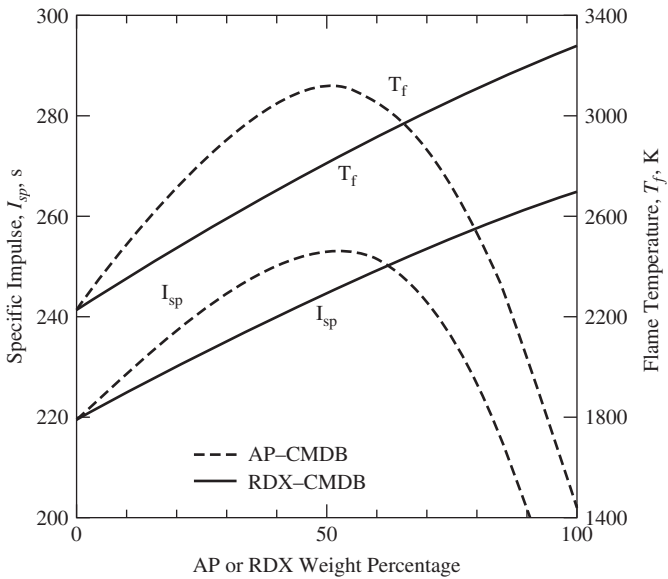


Figure 1.42 Variation of specific impulse and flame temperature with AP or RDX weight percentage of CMDB propellants (modified from Kubota, 1984).

TABLE 1.5. Thermochemical Properties of Several Propellant Oxidizers ($p_c = 70$ atm) (modified from Kubota, 1984).

Oxidizer	Chemical Formula	State	Density (g/cm ³)	ΔH_f (@ 298 K) (kcal/mol)	Product				
					T_g (K)	M_w (g/mol)	I_{sp} (s)		
NC (12.6%)	C ₆ H _{7.55} O ₅ (NO ₂) _{2.45}	S	1.66	-160.2	2586	24.7	230		
NC (14.14%N)	C ₆ H _{7.0006} N _{2.9994} O _{10.9987}	S	1.66	-155.99	3025	26.8	243		
NG	C ₃ H ₅ O ₃ (NO ₂) ₃	L	1.60	-9.75	3289	28.9	244		
TMETN	C ₅ H ₉ O ₃ (NO ₂) ₃	L	1.47	-97.8	2898	23.1	253		
TEGDN	C ₆ H ₁₂ O ₄ (NO ₂) ₂	L	1.33	-181.6	1376	19.0	183		
DEGDN	C ₄ H ₈ O ₃ (NO ₂) ₂	L	1.39	-103.5	2513	21.8	241		
AND	H ₄ N ₄ O ₄	S	1.82-1.84	-36.01	2051	24.8	202		
AN	NH ₄ NO ₃	S	1.73	-87.37	1247	22.9	161		
AP	NH ₄ ClO ₄	S	1.95	-70.73	1406	27.9	157		
HNF	CH ₅ N ₅ O ₆	S	1.87-1.93	-17.22	3082	26.4	254		
HNIW (CL-20)	C ₆ H ₆ N ₁₂ O ₁₂	S	2.04	+99.35	3591	27.4	273		
NP	NO ₂ ClO ₄	S	2.22	+8.88	597	36.4	85		
RDX	C ₃ H ₆ N ₃ (NO ₂) ₃	S	1.82	+14.69	3286	24.3	266		
HMX	C ₄ H ₈ N ₄ (NO ₂) ₄	S	1.90	+17.92	3278	24.3	266		
TAGN	CH ₉ N ₇ O ₃	S	1.59	-11.5	2050	18.6	231		

Major Combustion Products (Moles/Mole of Mixture)									
	O ₂	H ₂ O	CO	CO ₂	H ₂	N ₂	OH	HCl	Cl ₂
NC (12.6%)		0.226	0.418	0.127	0.116	0.111			
NC (14.14%)		0.249	0.349	0.192	0.061	0.135	0.007		
NG	0.069	0.280	0.107	0.275	0.014	0.181	0.041		
TMETN		0.263	0.357	0.096	0.140	0.136			
TEGDN		0.110	0.397	0.063	0.335	0.079			
DEGDN		0.253	0.365	0.079	0.190	0.111			
AND	0.196	0.399				0.397			
AN	0.143	0.571				0.286			
AP	0.287	0.377				0.119		0.197	0.020
HNF	0.099	0.334	0.021	0.123		0.348	0.036		
HNIW	0.019	0.135	0.237	0.138	0.027	0.366	0.036		
NP	0.750					0.125			0.125
RDX		0.226	0.246	0.082	0.089	0.326			
HMX		0.227	0.246	0.082	0.089	0.326			
TAGN		0.208	0.097	0.014	0.292	0.389			

and performance of several propellant oxidizers are shown in Table 1.5; similar parameters for common fuel binders are shown in Table 1.6.

Figure 1.43 shows the variations of combustion product molecular weight and flame temperature of various HTPB-based solid propellants with oxidizer weight percentage. As shown in Figure 1.44, NP shows the highest peak specific impulse

TABLE 1.6. Thermochemical Properties of Several Propellant Binders

Binder	Chemical Formula	ΔH_f^a (kJ/mol)	T_{glass} ($^{\circ}$ C)	Oxygen Balance ^b , %	Density (kg/m ³)	Impact Sensitivity (Nm)
PLN ^e	[C ₅ H ₉ NO ₄] _n	-334.7	-25 ^c	-114.3	1260	>9
PGN ^f	[C ₃ H ₅ NO ₄] _n	-284.5	-35 ^d	-60.5	1390-1450	>20
HTPB	[C ₁₀ H _{15.4} O _{0.07}] _n	-51.9	-63	-323.8	916	>50
GAP	[C ₃ H ₅ N ₃ O] _n	117.2	-50	-121.2	1300	16 → 120
BAMO ^g	[C ₅ H ₈ N ₆ O] _n	413.0	-39	-123.8	1300	>20

^aValues apply for $n = 1$.

^bThe oxygen balance is defined as the ratio of the mass of excess oxygen after a complete conversion of the oxidizer into oxides (with the exception of nitrogen oxides) and the mass of the oxidizer.

^cBy using suitable plasticizers for PLN, glass transition temperatures as low as -63° C have been obtained.

^dFor PGN, the glass transition temperature may be lowered substantially by using suitable plasticizers.

^ePLN: Poly-3-nitratomethyl-3-methyloxetane, also called POLYNIMMO or PN.

^fPGN: Polyglycidyl nitrate.

^gBAMO: 3,3'-Bis(azido methyl)oxetane.

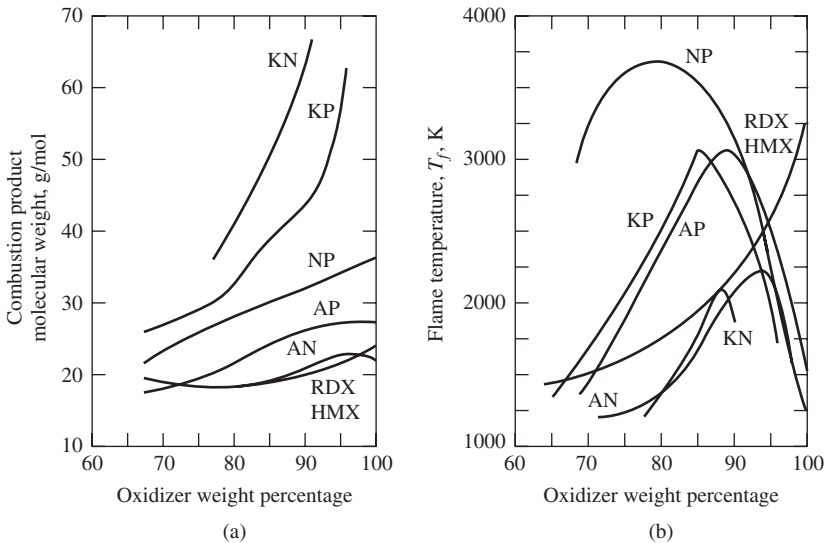


Figure 1.43 Variation of (a) molecular weight, and (b) flame temperature of several HTPB-based solid propellants with oxidizer concentration (modified from Kubota, 1984).

among several HTPB-based solid propellants; however, it is not a commonly used oxidizer since NP begins to decompose slowly at approximately 50° C, resulting in the production of gaseous products. There is some evidence that the purity of the sample is related to the decomposition. Despite efforts by several investigators to obtain high-purity samples, however, decomposition is significant

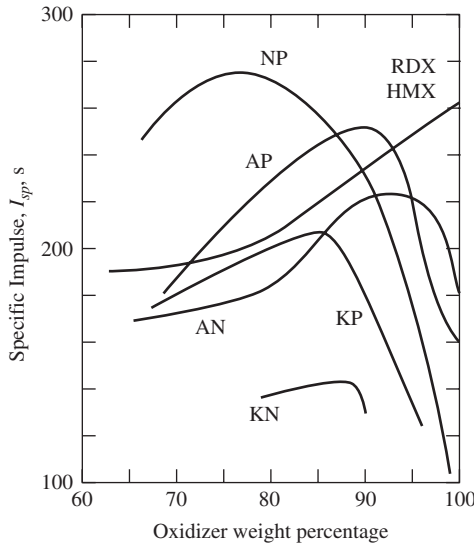


Figure 1.44 Variation of specific impulse of several HTPB-based solid propellants with oxidizer concentration ($p_c = 7$ MPa, $p_e = 0.1$ MPa) (modified from Kubota, 1984).

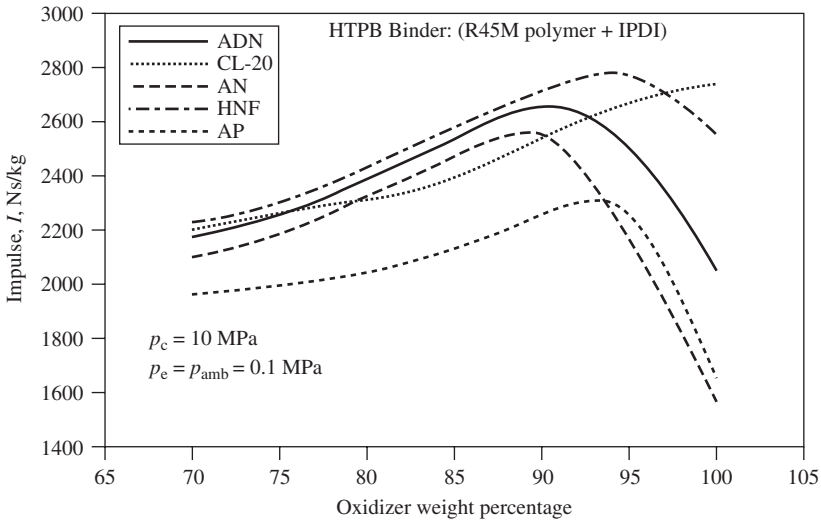


Figure 1.45 Variations of impulse of propellant with HTPB binder (R45M + IPDI) with various oxidizers and their weight percentages.

at temperatures above 60°C . This temperature is too low for practical propellant applications. Therefore, NP is not used as a usual propellant ingredient despite giving a very high I_{sp} . The variation in impulse of a HTPB binder (R45M+IPDI) with oxidizer wt% is shown in Figure 1.45 for many different oxidizers. These results are calculated by using the NASA-CEA code.

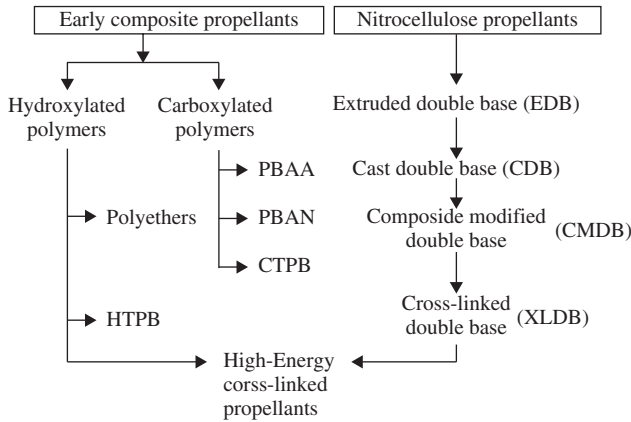


Figure 1.46 Family tree of double-base and composite propellants with high-energy cross-linked propellants (modified from Devanas, 2003).

Six major families of propellants are commonly manufactured and used (Devanas, 2003). They are shown in Figure 1.46 and described next.

1. Extruded double base (EDB) propellants which are more than 100 years old, are prepared by impregnation of NC with NG in water to obtain a paste. The most frequently employed NC has 12.6% nitrogen content. Solubility and ability to plasticize of an EDB propellant is a function of the nitrogen content. The final composition is obtained by kneading the mixture with additives, which include stabilizers, ballistic modifiers, flame suppressants, and others. The final configuration is obtained by extrusion through a die having the desired shape. The outer diameter is limited to about 300 mm. Long cylindrical shapes are obtained directly, but sometimes additional grain machining may also be performed.
2. The cast double-base (CDB) propellants ingredients are similar to those of EDB propellants. They are obtained by casting a mixture of NG and an inert plasticizer, called casting solvent, into a mold (which can be the rocket motor case) containing a previously prepared NC-based powder in which various additives already have been incorporated. The casting solvent swells and dissolves the NC through a curing of some days at elevated temperature (typically 60°C). CDB propellants have much less stringent size restrictions, and they allow the realization of three-dimensional shapes. Because EDB and CDB propellants are generally stiff, with a high elastic modulus and low elongation capability, especially at low temperatures, their use is rather limited to free-standing solid propellant grains.
3. Composite modified double-base (CMDB) propellants are derived from CDB propellants by the addition of energetic solids and NG, which increases the level of energy and the plasticization of the final formulation. When these propellants contain only nitramine (HMX or RDX) particles,

their atomic composition based on carbon (C), hydrogen (H), oxygen (O), nitrogen (N), gives them minimum smoke propellant. This name is given because there are very few condensed-phase species in the combustion products and no secondary condensation generated in the exhaust plume.

4. Elastomeric modified cast double-base (EMCDB) propellants, an improvement of CDB with better mechanical properties for case bonding, have been developed in the United Kingdom. They are produced by the same processes as CDB and CMDDB with the same basic formulations. A hydroxyl prepolymer (polyester, polycaprolactone) and an isocyanate cross-linking agent are introduced in the liquid casting solvent.
5. Composite propellants are based on a low-energetic polymeric binder and high levels of AP. They might or might not contain aluminum powder as a fuel. They are obtained by mixing the solids and liquid binder ingredients under vacuum conditions, introducing a cross-linking agent into this mixture, casting under vacuum conditions, and curing the cast sample to obtain a solid grain. The propellants without aluminum are called reduced smoke propellants because there is no primary smoke in the exhausts; ambient temperature and humidity secondary smoke formation is possible in certain conditions by condensation of water in the presence of hydrochloric gas resulting from the combustion of AP.
6. "High-energy propellants" is the name given to compositions based on a binder highly plasticized by a liquid nitric ester or a mixture of nitric esters and energetic solids, such as nitramines. They might also contain AP and aluminum powder. They are sometimes called cross-linked double base (XLDB) propellants even if there is very little or no NC in the binder. Their physical behavior is of the same type as composite propellants. Their production process is roughly the same, with a special preparation of the energetic binder elements. Composite and high-energy propellants are very well suited for case-bonded grain applications because of their mechanical behavior: They have a low modulus of elasticity and high-elongation capability in a wide temperature range.

Besides the main ingredients, all propellants can contain additives, generally at low contents, used as stabilizers, flame luminosity suppressants, combustion instability suppressants, and burning rate modifiers. One of the important tasks of propellants chemists is to find a practical way (e.g., using smaller particle size, burning rate modifier, etc.) to control the burning rate and pressure exponent, which are key factors in designing solid rocket motors (SRMs).

1.2.1.3 Density-Specific Impulse

The performance of tactical missiles is measured by the density- I_{sp} , which is defined as the product of propellant density and specific impulse; that is,

$$DI_{sp} \equiv \rho I_{sp} = \rho_p \times I_{sp} \quad (1.60)$$

In order to accommodate a large weight of propellant in a given combustor volume, a dense propellant is preferred. This permits smaller vehicle size and weight, which also results in lower aerodynamic drag. The average propellant density has an important effect on the maximum flight velocity and range of any rocket-powered propulsion systems. The average propellant density can be increased by adding heavy materials such as aluminum powders into the propellant mixture. A comparison of three propulsion systems is shown in Table 1.7.

Due to their inherent safety feature and flexibility in thrust profiling, hybrid rockets have many advantages over solid propellant rockets. They should be considered in the development of future propulsion systems.

The delivered specific impulses and densities of the six propellant families are summarized in Figure 1.47. The values shown are measured in standard rocket motors. In the United States, the standard testing rocket motor is called the Ballistic Test and Evaluation System (BATES). A description of the BATES motor can be found in the literature (Geisler and Beckman, 1998). To make comparisons, standard conditions of operation of the motor must also be defined. The most important operating conditions are the chamber pressure and the expansion ratio.

TABLE 1.7. Comparison of Several Propulsion Systems

Propulsion System	I_{sp} (s)	$D \cdot I_{sp}$ (g-s/cm ³)
Liquid bi-propellant rockets	260-410 (LOX/H ₂ : 390)	100-430 (LOX/H ₂ : 100)
Hybrid rockets	280-380 (LOX/HTPB: 330)	300-520 (LOX/HTPB: 350)
Solid propellant rockets	190-270 (AP/Binder/Al: 270)	290-470 (AP/Binder/Al: 470)

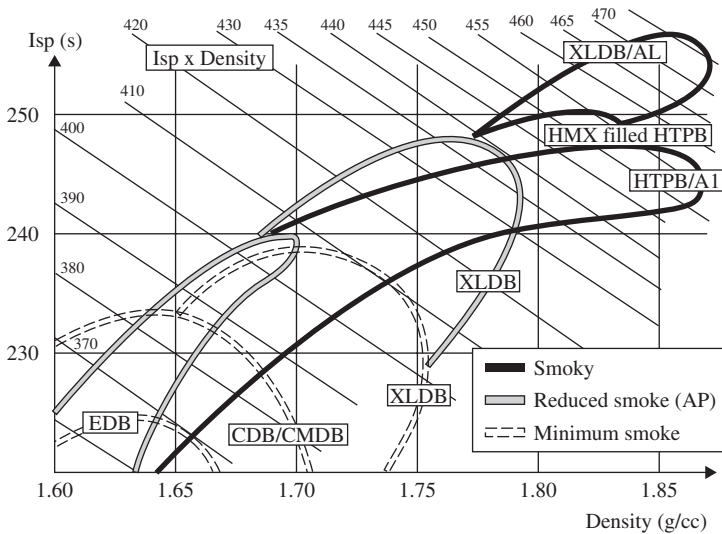


Figure 1.47 Delivered I_{sp} versus densities of main propellant families (modified from Devanas, 2003).

In Figure 1.47, these values are 7 MPa and an expansion from 7 to 0.1 MPa. Other standard motors and operating conditions are described in the literature; however, sometimes the calculated values neglect all losses, especially two-phase flow losses resulting from condensed solids, such as alumina.

1.2.1.4 Effective Vacuum Exhaust Velocity

The specific impulse of a rocket motor, calculated by assuming that the rocket exhausts into the vacuum, is called the vacuum-specific impulse ($I_{sp,vac}$). The effective vacuum exhaust velocity can be determined by multiplying the vacuum-specific impulse by the gravitational acceleration as shown by

$$V_{e,vac} \text{ [m/s]} \equiv I_{sp,vac} \text{ [s]} \times g_0 \text{ [m/s}^2\text{]} \quad (1.61)$$

Some sources provide the vacuum-specific impulse in terms of the effective vacuum exhaust velocity given in the units of [m/s].

1.2.1.5 Characteristic Velocity C^*

A characteristic velocity C^* is defined as a measure of energy after the combustion of propellant that can be used to generate thrust. It is defined as:

$$C^* \equiv \frac{\int_{t_0}^{t_E} p_c A_t dt}{M_p} \quad (1.62)$$

If the chamber pressure is constant for major part of the rocket operation, then C^* can be written in this algebraic form:

$$C^* = \frac{p_c A_t}{\dot{m}_p} = \frac{\sqrt{R_u}}{\Gamma} \sqrt{\frac{T_c}{Mw}} = \frac{1}{C_D} \quad (1.63)$$

The characteristic velocity C^* is a fundamental performance parameter, which is similar to the I_{sp} . Both of these parameters are directly proportional to $\sqrt{T_c/Mw}$. Typical values for C^* range from 800 to 1,800 m/s. Higher values of C^* correspond to more energetic propellants, which can produce greater thrust and impulse. Using the definition of C^* , thrust can be expressed as:

$$F = \dot{m}_p C_F C^* \quad (1.64)$$

For a nonmetallized AP/HTPB composite propellant burning at a pressure of 70 bar, the calculated characteristic velocity is shown in Figure 1.48 as a function of AP weight percentage. This plot shows that the solid loading of AP should be approximately 88% for maximum performance.

For a metallized AP/HTPB/Al composite propellant burning at a pressure of 70 bar, the calculated characteristic velocity is shown in Figure 1.49 as a function of Al weight percentage. This plot indicates that the upper limit for Al powder is near 18% by weight.

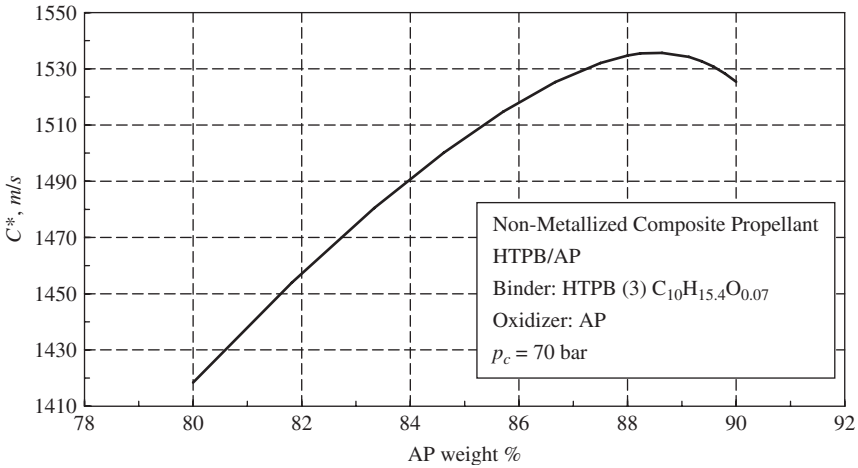


Figure 1.48 C^* as a function of AP weight percentage.

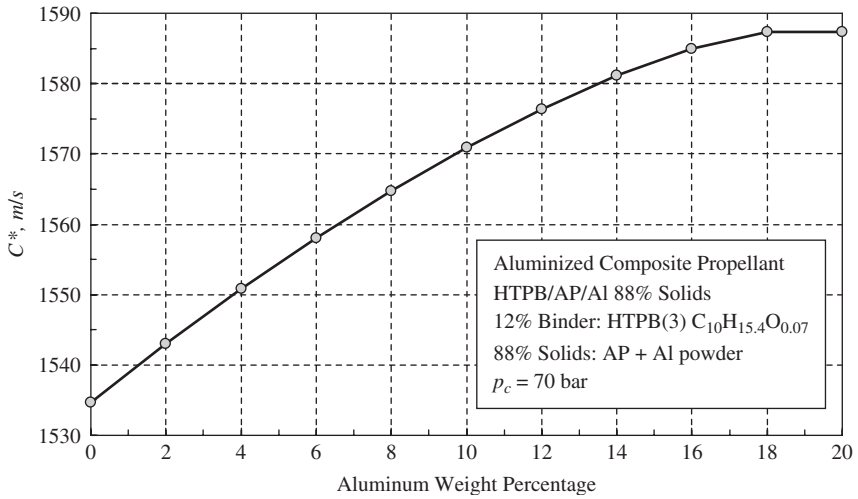


Figure 1.49 C^* as a function of aluminum weight percentage.

1.2.1.6 Pressure Sensitivity of Burning Rate

The parameter K_n is defined as the ratio of the instantaneous burning surface area of the solid propellant grain to the instantaneous nozzle throat area of a rocket motor; that is,

$$K_n \equiv A_b/A_t \tag{1.65}$$

The pressure sensitivity π_k of the rocket motor combustor is defined as

$$\pi_k \equiv \frac{1}{P} \left[\frac{\partial P}{\partial T_i} \right]_{K_n} \tag{1.66}$$

π_k represents the percentage of change of chamber pressure with respect to the initial temperature of the propellant while keeping the K_n value constant. The pressure in the solid-propellant rocket motor combustion chamber can be expressed as:

$$p = p_{ref} e^{\pi_k (T_i - T_{i,ref})} \quad (1.67)$$

Therefore, the pressure sensitivity of a rocket motor can be written as:

$$\pi_k = \frac{\ln(p/p_{ref})}{(T_i - T_{i,ref})} \quad (1.68)$$

The relationship between the temperature sensitivity σ_p defined in Equation 1.30 and π_k is given by the next equation with the pressure exponent n treated as a constant:

$$\sigma_p = (1 - n) \pi_k \quad (1.69)$$

1.2.1.7 Thrust Coefficient Efficiency

In the theoretical calculations of the thrust coefficient ($C_{F,th}$), nozzle throat erosion rate is assumed to be zero. However, under experimental conditions, the nozzle throat size may increase due to thermochemical and/or mechanical erosion. The experimental value of C_F can be evaluated from the next equation:

$$C_{F,ex} \equiv \frac{\int_{t_0}^{t_E} F(t) dt}{\int_{t_0}^{t_E} A_t(t) p_c(t) dt} \quad (1.70)$$

The instantaneous thrust, chamber pressure, and throat area could be measured for calculating the $C_{F,ex}$. The theoretical thrust coefficient $C_{F,th}$ can be determined from Equation 1.46. The average thrust-coefficient efficiency or thrust efficiency is then defined as:

$$\eta_{C_F} \equiv \frac{C_{F,Experimental}}{C_{F,Theoretical}} = \frac{C_{F,ex}}{C_{F,th}} \quad (1.71)$$

1.2.1.8 Effect of Pressure Exponent on Stable/Unstable Burning in Solid Rocket Motor

The burning-rate pressure exponent has a very strong effect on the stability of a solid rocket motor. This can be visualized from the mass balance equation in the rocket motor combustor. The mass discharge rate from the rocket motor is directly proportional to chamber pressure; that is, $\dot{m}_d \propto p_c$, based on Equation 1.49. The mass generation rate from the propellant combustion is proportional to p_c^n ; that is, $\dot{m}_g \propto p_c^n$, based on Equation 1.48. If $n > 1$, then any pressure fluctuation in the motor will lead either to overpressure in the motor or to a dramatic decrease in chamber pressure resulting in extinction of the solid-propellant

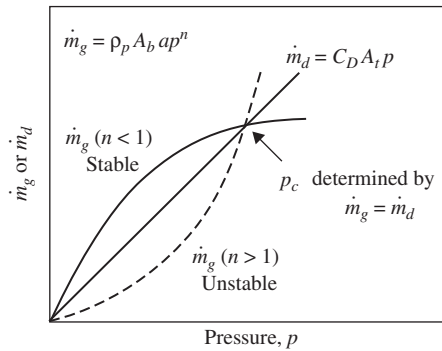


Figure 1.50 Effect of burning-rate pressure exponent on stability of solid rocket motor (Kubota, 1984).

combustion process. Thus, the solid propellants for rocket motors should have $n < 1$. This can be seen from Figure 1.50. The intersection point of the solid straight line representing \dot{m}_d and a dashed curve representing \dot{m}_g with $n > 1$ shows the equilibrium condition in the rocket motor. A small increase in the chamber pressure will result in further increase of chamber pressure, thus leading to overpressurization of the rocket motor combustor. A small reduction in the chamber pressure will result in continuous decrease in the chamber pressure, thus resulting in extinction of solid-propellant combustion. If $n < 1$, however, the mass generation rate is represented by the solid curve. A small reduction in the chamber pressure will reduce the mass generation rate, but it would be higher than the mass discharge rate; therefore, the chamber pressure will continue to increase toward the equilibrium point. Similarly, if the instantaneous chamber pressure is increased slightly, then the mass discharge rate will be higher than the mass generation rate; thus the chamber pressure will reduce toward the equilibrium pressure. Therefore, the burning rate pressure exponent must be less than 1. This unstable burning with $n > 1$ is different from the low-pressure deflagration limit (PDL) of a solid propellant, below which the flame cannot sustain burning.

1.2.2 Performance Parameters of Solid-Propellant Gun Systems

The main purpose of a gun is to impart energy to the projectile to reach a certain high velocity, called muzzle velocity, before the projectile leaves the gun. The wall and the breech of the gun are to hold the pressure of the gas during the projectile acceleration. The length of a gun is measured from breech face to the muzzle; often it is expressed in terms of caliber. For example, a 6-in, 36-caliber gun has a length of 36×6 in, or 18 ft. The internal diameter of the bore is called caliber. There are three types of artillery systems: (1) guns that have tube lengths longer than 30 calibers; (2) howitzers, which are guns with tube lengths of 20 to 30 calibers; and (3) mortars, which are systems with tube length between 14 and 17 calibers. Since solid propellants are used in many gun propulsion systems, we must discuss some gun barrel structures before defining

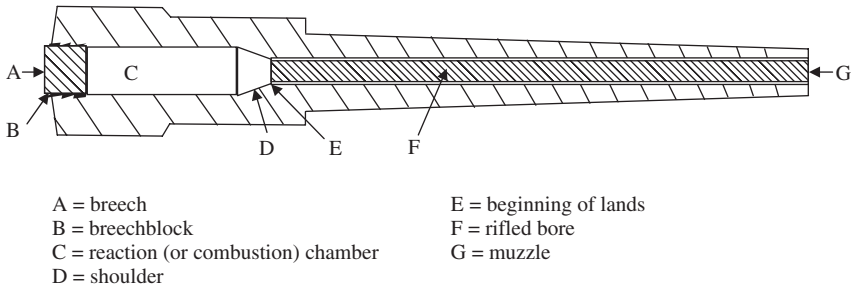


Figure 1.51 Typical gun barrel design with nomenclature (from Army Material Command Pamphlet AMCP 706–252, 1964).

the key performance parameters. Figure 1.51 is a cross-sectional view of a typical gun barrel with nomenclature.

A gun system contains a projectile and a projectile guiding tube connected to a combustion chamber (also called a reaction chamber). The burning of solid propellant contained in the combustion chamber transforms the chemical energy into thermal energy. This process generates hot combustion products and pressurizes the reaction chamber rapidly. Because the initial resistance to projectile motion is quite high, relatively large chamber pressures are attained before significant projectile motion has occurred. Subsequently, the projectile moves along the gun tube causing the combustion products to expand and push the projectile through the gun tube at very high velocity. Some gun systems have helix-shaped pattern in the barrel of a gun, which is called a rifled gun tube. Rifling imparts some spin to the projectile around its axis. Some of the kinetic energy of the projectile is used by its spinning motion in the rifled bore region of a gun tube. The volume of the reaction chamber increases due to the projectile motion, and the chamber pressure reduces. However, since the burning rate of solid propellant is a strong function of pressure, the high pressure generated before the projectile motion causes the solid propellant to burn more rapidly. These two effects compete with each other so that a rapid pressure increase is observed until the pressure reaches a peak value, after which the pressure starts to decrease. The typical peak pressure in gun systems could be approximately 700 MPa. The typical muzzle velocity could be 900 m/s for a gun system. Usually the performance of a gun system is described in terms of pressure and projectile velocity variation with the projectile travel distance in the gun tube. These curves are called pressure-travel and velocity-travel curves, respectively. Figure 1.52 shows four pressure-travel curves (p_1 , p_2 , p_3 , and p_4) and one velocity-travel curve (V_p). As shown in Equations 1.72 and 1.73, the area under the pressure-travel curve indicates the work performed on the projectile.

$$\text{Area under pressure-travel} = \frac{\text{Work on projectile}}{\text{Unit cross-sectional area}} \quad (1.72)$$

$$\int p ds = \frac{\text{Work}}{\text{Unit area}} \quad (1.73)$$

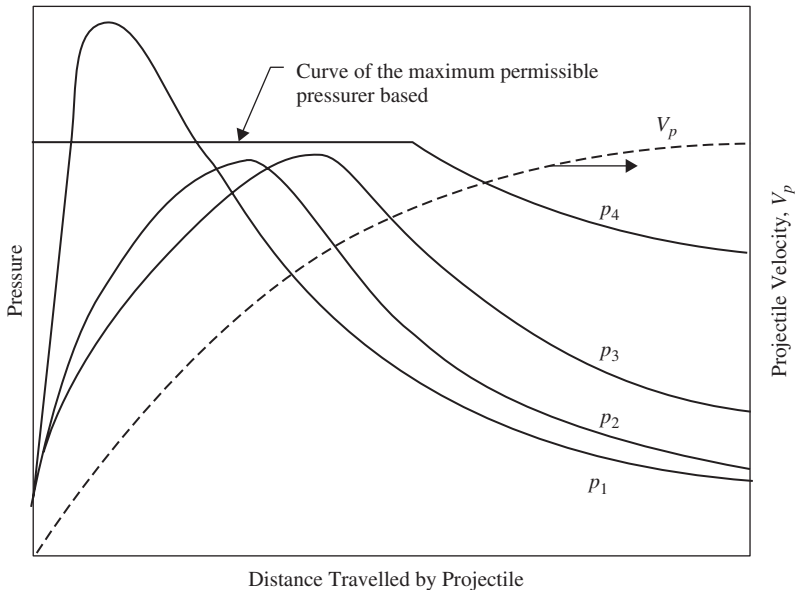
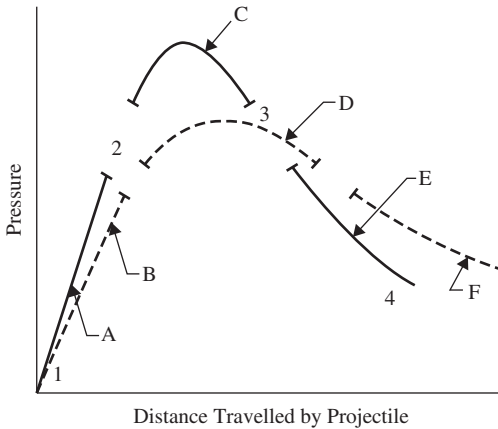


Figure 1.52 Typical pressure-travel and velocity-travel plot for a gun system (modified from Krier and Adams, 1979).

The curve p_4 corresponds to the maximum pressure that is permissible for maintaining the structural integrity of the gun tube. In order for a pressure-travel curve to be acceptable, the curve should lie below the p_4 curve. The curves p_1 and p_2 have equal areas under them, which indicates that the work performed on the projectile in both cases is equal. However, the curve p_1 is unacceptable since it exceeds p_4 . The area under p_3 is greater than that of p_2 ; thus, more work is done on the projectile. Since the work done on the projectile is realized as kinetic energy, we can conclude that higher work on the projectile results in higher projectile velocity (V_p). A higher pressure curve than p_3 is allowed as long as it does not exceed p_4 . However, erosion of gun barrel should also be considered to make the system more durable.

The characteristic pressure-travel curve of a gun system depends on several parameters, including the strength of solid-propellant ignition system, the exposed surface area of the propellant grains, the burning rate of the propellant, projectile weight, projectile resistances to linear and rotational motion, and environmental factors.

Figure 1.53 shows the influence of these parameters on the pressure-travel curve. The slope of curve in the region 1–2 is affected primarily by the ignition and combustion characteristics of the gun system. The shape of the curve in region 2–3 is governed by propellant grain configuration. The region 3–4 is dominated by the propellant burning rate, the projectile weight, and the rotational resistance to the projectile in the rifled bore section. The effect of propellant



- A = Strong ignition (high initial burning surface area)
- B = Weak ignition (low initial burning surface area)
- C = Rapid change in burning surface area (many perforations or small granular particles)
- D = Less rapid change in burning surface area (fewer perforations or larger granular particles)
- E = Rapid chamber expansion (lighter projectile, lesser rotational resistance)
- F = Less rapid chamber expansion (heavier projectile, greater rotational resistance)

Figure 1.53 Parameter influence on pressure-travel curves (modified from Krier and Adams, 1979).

grain (or granular particles) parameters on the pressure-travel curves is shown in Figure 1.54.

Some typical propellant grain configurations are shown in Figure 1.55. These configurations are very significant for application purposes. Some of these grains are regressive (if their burning surface area decreases with time); some are progressive (if their burning surface area increases with time). The neutral grain configuration corresponds to the constant burning surface area. If the exposed burning surface of a given propellant grain is assumed to regress uniformly, then the burning surface area versus the fraction of grain burned can be evaluated as a form function to determine its progressive or regressive nature. Usually the multiperforated grains are progressive, the tubular grain is neutral, and all others grains are regressive.

1.2.2.1 Energy Balance Equation

Consider a thermodynamic system consisting of solid propellant, a gun tube, and a projectile, as shown in Figure 1.56. In this simplified system, it is assumed that all of the solid-propellant material is consumed before the projectile motion at the thermodynamic state 1. Once the projectile reaches the end of the gun tube before exiting the muzzle, it is in thermodynamic state 2. From the first

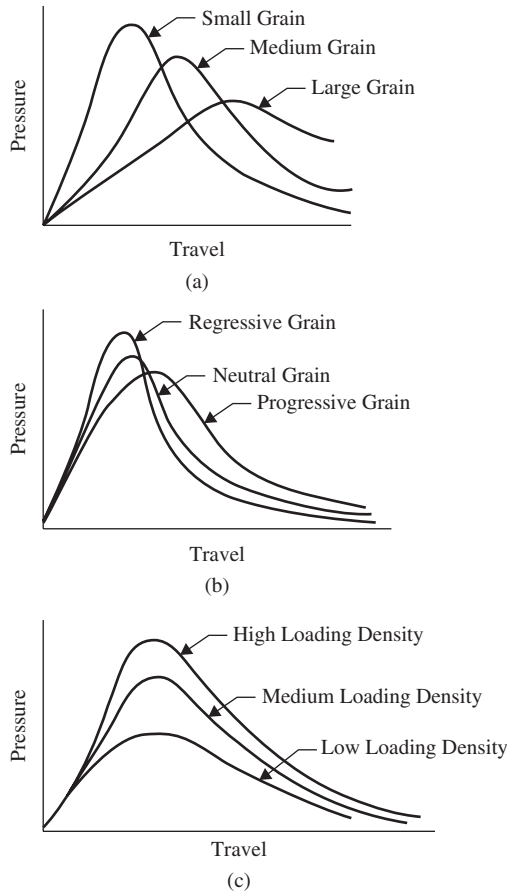


Figure 1.54 Propellant grain parameters (a) propellant size, (b) grain configuration, and (c) loading density (Δ) effect on pressure-travel curves (modified from Krier and Adams, 1979).

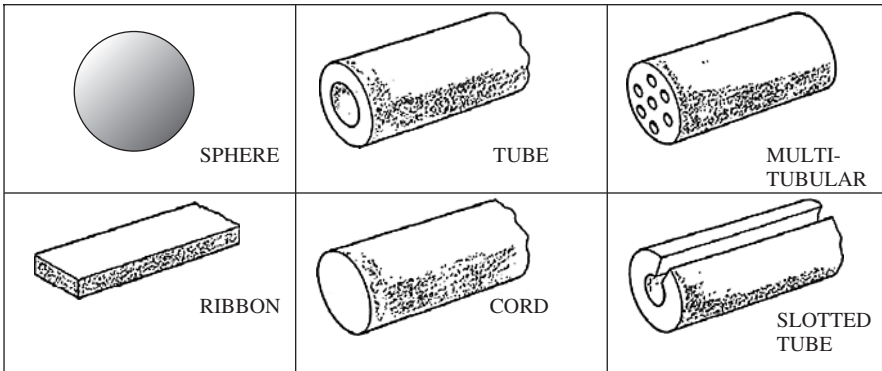


Figure 1.55 Various propellant grain configurations.

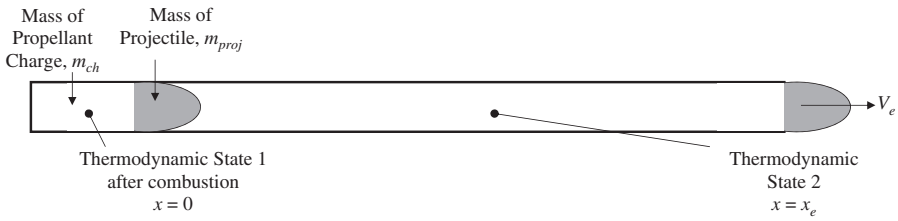


Figure 1.56 Description of two thermodynamic states in the gun tube.

law of thermodynamics, the energy balance for the thermodynamic system (consisting of the products generated by combustion of propellant charge) between states 1 and 2 can be written as:

$$\underbrace{{}_1Q_2}_{= 0 \text{ if there is no heat loss to tube}} = \underbrace{U_2 - U_1}_{= m_g C_v (T_2 - T_1)} + m_g (V_2^2 - V_1^2) / 2 + \underbrace{m_g g (z_2 - z_1)}_{= 0} + \underbrace{{}_1W_2}_{\text{Work performed by gas on projectile}}$$

(1.74)

If the kinetic energy of the gases at state 2 is much smaller than the change in internal energy of gases, then

$$m_g C_v (T_1 - T_2) \approx {}_1W_2 \quad \text{Note that: } {}_1W_2 = \int_0^{x_e} p A dx = \frac{1}{2} m_{proj} V_e^2 \quad (1.75)$$

where V_e is the muzzle velocity of the projectile.

For polytropic expansion processes, we have;

$$p \mathcal{V}^n = \text{constant} \quad (1.76)$$

When the process is isentropic, then $n = \gamma$, where γ is the ratio of specific heats $= C_p / C_v$. The work done by the expanding gases on the moving boundary (i.e., the projectile) during expansion process is:

$${}_1W_2 = \int_1^2 p d\mathcal{V} = \text{constant} \int_1^2 \frac{d\mathcal{V}}{\mathcal{V}^\gamma} = \frac{p_2 \mathcal{V}_2 - p_1 \mathcal{V}_1}{1 - \gamma} \quad (1.77)$$

Assuming the ideal gas law ($pV = mRT$) can be applied to this case, and assuming it is a closed system (i.e., the gaseous mass $m = \text{constant}$ between state 1 and state 2), then we have:

$${}_1W_2 = \frac{mR(T_2 - T_1)}{1 - \gamma} \quad (1.78)$$

The pressure in the gun chamber changes with the projectile travel. Therefore, a mean pressure during the projectile travel can be defined as:

$$p_{mean} \equiv \frac{1}{x_e} \int_0^{x_e} p dx \quad (1.79)$$

where x_e is defined the physical distance between the state 1 and state 2. In terms of the mean pressure, the work done on the projectile by the combustion product gases is equal to its kinetic energy in the absence of any other energy losses:

$${}_1W_2 = \int_0^{x_e} p A dx = p_{mean} A x_e = \frac{1}{2} m_{proj} V_e^2 \quad (1.80)$$

In reality, a portion of gaseous mass moves along with the projectile at the same velocity as that of the projectile. Therefore, the effective mass of the projectile is often expressed as the sum of projectile mass and a portion of propellant charge mass:

$$m_e = m_{proj} + \varepsilon m_{ch} \quad (1.81)$$

where ε is the portion of the gases traveling with the projectile ($\varepsilon \leq 0.5$). Therefore, Equation 1.80 can be rewritten as:

$${}_1W_2 = p_{mean} A x_e = \frac{1}{2} m_e V_e^2 \quad (1.82)$$

1.2.2.2 Efficiencies of Gun Propulsion Systems

Two particular parameters are commonly employed to quantify the overall propulsive performance in a particular gun-charge-projectile system: piezometric efficiency, η_p , and ballistic efficiency, η_b . The piezometric efficiency (η_p) is defined as the ratio of mean pressure and the maximum breech pressure given in Equation 1.83. The mean pressure is defined by Equation 1.79.

$$\eta_p \equiv \frac{p_{mean}}{p_{max}} \quad (1.83)$$

In general, a higher piezometric efficiency corresponds to a flatter pressure-travel curve. Before defining the ballistic efficiency, it is useful to define a key parameter known as impetus of a gun propellant (I_m). It represents the energy available from combustion of the propellant per unit mass of the propellant. It is defined as

$$I_m \equiv RT_f = R_u T_f / M_w \quad \text{Unit} = (\text{MJ/kg} \quad \text{or} \quad \text{J/g}) \quad (1.84)$$

In order to achieve high impetus, low-molecular-weight combustion products combined with high flame temperature would be beneficial. However, to avoid gun barrel erosion, we cannot have very high flame temperatures, like those for rocket propellants.

The ballistic efficiency (η_b) can be defined as the ratio of total work done on the projectile to the total work potential of the propelling charge. Thus, an expression for ballistic efficiency can be written as:

$$\eta_b \equiv \frac{\frac{1}{2}m_e V_e^2}{m_{ch} C_v T_f} = \frac{\frac{1}{2}m_e V_e^2 (\gamma - 1)}{m_{ch} R T_f} = \frac{\frac{1}{2}m_e V_e^2 (\gamma - 1)}{m_{ch} I_m} \quad (1.85)$$

where m_{ch} is the propellant charge mass and I_m is the impetus. A high ballistic efficiency can be obtained by burning the propellant charge as early as possible during the projectile's travel in the gun bore. In this manner, the residual muzzle pressure can be minimized.

Another important performance parameter for a gun propulsion system is thermal efficiency. By using the definition of piezometric efficiency, the work done on the projectile by the product gases of solid propellants can be written as

$${}_1W_2 = \int_0^{x_e} p A dx = p_{mean} A x_e = p_{max} \eta_p A x_e \quad (1.86)$$

Using Equations 1.82 and 1.86, we have

$$p_{max} = \frac{m_e V_e^2}{2A x_e \eta_p} = \frac{(m_{proj} + \varepsilon m_{ch})}{2A x_e \eta_p} V_e^2 \quad (1.87)$$

The *thermal efficiency* of this gun system can be defined as

$$\eta_{th} = \frac{\frac{1}{2}m_{proj} V_e^2}{m_{ch} \Delta H_{ex}^o} \quad (1.88)$$

where ΔH_{ex}^o represents the heat of explosion per unit mass of propellant. If the effective mass of projectile is considered, then the efficiency is called the characteristic coefficient (ζ_e) and is defined as:

$$\zeta_e \equiv \frac{\frac{1}{2}m_e V_e^2}{m_{ch} \Delta H_{ex}^o} \quad (1.89)$$

The muzzle velocity (V_e) of the projectile can be written in terms of the characteristic coefficient and the mass ratio of propellant charge and projectile as shown next:

$$V_e = \sqrt{\frac{2\zeta_e \Delta H_{ex}^o}{\left(\frac{m_{proj}}{m_{ch}} + \varepsilon\right)}} \quad (1.90)$$

The relationship between the muzzle velocity and the mass ratio of propellant charge and projectile is shown in Figure 1.57. The muzzle velocity has a maximum asymptotic value of 2,400 m/s for the conventional gun propellants.

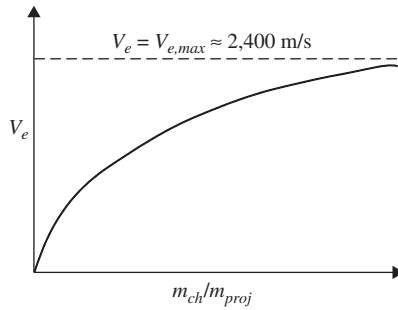


Figure 1.57 Relationship between muzzle velocity and the mass ratio of propellant charge and projectile.

1.2.2.3 Heat of Explosion (ΔH_{ex}^o)

The heat of explosion ΔH_{ex}^o of an explosive or propellant material is the heat liberated during its explosive decomposition and burning. Its magnitude depends on the thermodynamic state of the combustion products. In general, water is considered in form of vapor in combustion products. The calculations are based on the assumption that the carbon, hydrogen, nitrogen, and oxygen of the solid propellant are transformed into CO or CO₂, H₂, water vapor, and N₂. It is assumed that no free oxygen or dissociation exists. Under these assumptions, the heat of explosion of a given propellant can be calculated from Equation 1.91.

$$\Delta H_{ex}^o \left[\frac{\text{kcal}}{\text{g}} \right] = \frac{(-\Delta H_c^o \left[\frac{\text{kcal}}{\text{mol}} \right]) - 67.421 \left[\frac{\text{kcal}}{\text{g-atoms}} \right] \{ (2C + 0.5H - O) \left[\frac{\text{g-atoms}}{\text{mol}} \right] \}}{Mw_{propellant} \left[\frac{\text{g}}{\text{mol}} \right]} \quad (1.91)$$

The heat of combustion and heat of explosion for several major propellant ingredients is given in Table 1.8.

TABLE 1.8. Heat of Combustion and Explosion of Several Propellant Ingredients

Substance	State	ΔH_c^o (kcal/gm)	ΔH_{ex}^o (kcal/gm)
NC (12.6% N)	Solid	-2.406	0.860
NG	Liquid	-1.616	1.480
TMETN	Liquid	-2.540	1.236
TEGDN	Liquid	-3.428	0.357
DEGDN	Liquid	-2.792	1.160
RDX	Solid	-2.285	1.439
HMX	Solid	-2.300	1.222
EC	Solid	-8.409	—
DBP	Liquid	-5.526	—

TABLE 1.9. Energy Distribution for a Medium-Caliber Gun

Energy Absorbed	Percentage of Total
1. Translation of projectile	
Rotation of projectile	32.00
Frictional losses	0.14
Subtotal of work done on projective (area under pressure-travel curve)	<u>2.17</u> 34.31
2. Translation of recoiling parts	0.12
Translation of propelling gases	3.14
Heat loss to gun and projectile	20.17
Sensible and latent heat losses from gases	<u>42.26</u>
Total propellant potential	100.00

It is beneficial to know the energy utilization of a gun propellant during its ballistic cycle. Table 1.9 lists the percentage of energy from the total propellant potential. The translational energy of the projectile in a medium-caliber gun is the main output from the propellant combustion. This amount is only 32%. This is a typical representation of the thermal efficiency of a gun system.

1.2.2.4 Relative Quickness, Relative Force, and Deviations in Muzzle Velocity

In order to achieve high reproducibility in muzzle velocity, it is important to compare the combustion behavior of the production lot of propellant with that of the standard lot of propellant in closed bomb tests. In the closed bomb tests, a low-loading density (<0.3 g/cc) of the propellant grains is utilized in a high-pressure closed vessel. The pressure-time traces are recorded for each test. The combustion performance of the production lots are compared to the standard lot in terms of relative quickness (RQ) and relative force (RF). These two parameters are defined as

$$RQ \equiv \frac{1}{N} \sum_{i=1}^N \frac{(dp/dt)_{(\text{@Prescribed pressures})}^{\text{test}}}{(dp/dt)_{(\text{@Prescribed pressures})}^{\text{std}}} \quad (1.92)$$

$$RF \equiv [p_{\text{max}}]^{\text{test}} / [p_{\text{max}}]^{\text{std}} \quad (1.93)$$

In Equation 1.92, the dp/dt values in both the numerator and denominator are measured at the same prescribed instantaneous pressures, $p_{\text{prescribed}}$. The parameter N is the total number of measurements made in a single test. Typically, N is equal to 4, as there are four equally spaced pressures in the middle of the pressure interval.

The muzzle velocity usually is correlated to RQ by this relationship:

$$V_e = a + bRQ \quad (1.94)$$

where a and b are correlation coefficients. The deviation in muzzle velocity from that of the standard lot can be related to the deviations in RQ and RF by this relationship:

$$\Delta V_e = a' \times \Delta RQ + b' \times \Delta RF \quad (1.95)$$

where a' and b' are two separate correlation coefficients.

1.2.2.5 Dynamic Vivacity

Dynamic vivacity is a useful parameter for determining the change of propellant burning surface area due to formation of cracks in the sample. The cracks could be formed in the propellant due to thermal aging or due to mechanical stress loading. The dynamic vivacity is defined as

$$\mathcal{L}(t) \equiv \frac{1}{p_{\max}} \frac{\partial \ln p(t)}{\partial t} \quad (1.96)$$

The dynamic vivacity depends on the instantaneous propellant burn rate, propellant surface area, chamber pressure, maximum chamber pressure, loading density, propellant density, and covolume of its product gases. Vivacity is sensitive to the propellant composition and actual propellant surface area. The dimension of vivacity is 1/(MPa-s).

CHAPTER PROBLEMS

1. From their molecular structure, determine the oxygen balance of these ingredients: HMX, TMETN, BTTN, and ADN.
2. Derive a steady-state temperature profile in the burning solid propellant from its original heat conduction equation given in Equation 1.5.
3. Plot thrust as a function of chamber pressure normalized by ambient pressure for an area ratio (nozzle exit to nozzle throat) of 20. Consider the γ value to be 1.25 and ambient pressure is to be 1 atm. Also plot the thrust coefficient versus P_c/P_{amb} for these parameters. The divergence angle α_d can be taken to be 15 degrees.
4. Plot the thrust coefficient as a function of area ratio by using the same parameters given in problem 3. Use $p_c/p_e = 15, 30, 45, 90$.
5. What are the relative magnitudes of various terms in Equation 1.74 for a typical gun system with bore diameter of 7.6 mm?